UC Santa Cruz
UC Santa Cruz Electronic Theses and Dissertations

Title

A ~3000 Year Multi-Proxy Paleoclimate Record from the Guaymas Basin, Gulf of California

Permalink

https://escholarship.org/uc/item/3df8c61w

Author

Stewart, Zach W.

Publication Date

2017

Supplemental Material

https://escholarship.org/uc/item/3df8c61w#supplemental

Peer reviewed|Thesis/dissertation

UNIVERSITY OF CALIFORNIA

SANTA CRUZ

**A ~3000 YEAR MULTI-PROXY PALEOCLIMATE RECORD FROM THE
GUAYMAS BASIN, GULF OF CALIFORNIA**

A thesis submitted in partial satisfaction of

the requirements for the degree of

MASTER OF SCIENCE

in

OCEAN SCIENCES

By

ZACH STEWART

June 2017

The thesis of Zach Stewart
is approved by:

_____
Professor Christina Ravelo

_____
Professor Matthew McCarthy

_____
Professor Ivano Aiello

_____
Tyrus Miller
Vice Provost and Dean of Graduate Studies

TABLE OF CONTENTS

Abstract

**A ~3000 YEAR MULTI-PROXY PALEOCLIMATE RECORD FROM THE
GUAYMAS BASIN, GULF OF CALIFORNIA**

Zach Stewart

The Guaymas Basin, Gulf of California, is an important site for
paleoclimate study due to ideal preservation conditions and high sedimentation
rates, which allow for high-resolution analysis of paleoclimate records and
investigation of climatic and oceanographic processes that operate over
timescales not resolved by modern instrumental records. Furthermore, the
Guaymas Basin receives some water advected at depth from the Eastern Tropical
North Pacific (ETNP), a region where oceanographic processes are closely
coupled to the global climate system. The past climate and oceanography of the
Gulf of California and ETNP have been well studied at low resolution over
glacial-interglacial timescales: the goal of this study is to elucidate Mid- to Late
Holocene oceanographic and climate changes at a higher resolution than
previous studies in order to resolve decadal to centennial variance. Three main
conclusions can be drawn from the new high-resolution records presented here.
First, a careful comparison of radiocarbon dating and layer counting data calls
into question the completeness of varved marine sequences in the Guaymas
Basin. Second, stable isotopes, elemental composition data, XRF core scan trace

metal counts, and smear slide analysis are used to identify a significant change in mean conditions and ecosystem structure at ~2800 yr BP, which is probably driven by southward displacement of the Inter-tropical Convergence Zone (ITCZ). Notably, mean bulk $\delta^{15}N$ is ~0.6‰ lower after 2800 yr BP, suggesting decreased denitrification and improved ventilation. Third, important frequencies of variance at centennial and decadal periodicities are identified. Comparison of these new high-resolution proxy records to previous work in other regions suggests that Mid- to Late Holocene changes in the Guaymas Basin may be linked to climate changes across a larger spatial scale.

Acknowledgements

1. Introduction

In the context of recent anthropogenic climate change, it is especially important to understand variability in the ocean-climate system on a timescale relevant to human societies. Instrumental records of climate change are too short to detect decadal to century scale variability, and many paleoclimate records lack the resolution necessary to investigate short timescale variability. High-resolution records like the one presented here have the potential to extend understanding of climate and oceanographic change over these timescales. The Gulf of California is a highly productive coastal upwelling region, has a well-developed Oxygen Minimum Zone (OMZ), excellent preservation of laminated sediments, and is located in a region with important modern and paleo human populations. The Gulf of California is of special importance because it exchanges waters with the ETNP, a region known to be important in the global climate system (Deutsch et al., 2001; Altabet et al., 1995). This study aims to document changes in ecosystem structure, productivity, and climate in the Guaymas Basin, Gulf of California, over the Mid- to Late- Holocene, and also considers how these changes may be related to events in the ETNP and global climate systems.

Because of ideal preservation conditions and the importance of paleoceanographic records from this region, several studies are published from the Central Gulf of California. Pride et al. (1999) used nitrogen isotopes to investigate global climate change response in the Central Gulf on glacial-

interglacial time scales, but did not focus on the Late Holocene, which is most relevant to changes in the development of Maya society in the region. Barron et al. (2004, 2005) produced a ~15,000-year paleoclimate record, using diatoms, coccoliths, and silicoflagellate microfossils to interpret an increase in siliceous productivity and ENSO variability in the Guaymas Basin at 2800 yr BP. Perez-Cruz (2013) investigated changes in precipitation, paleoproductivity, and Inter-Tropical Convergence Zone (ITCZ) position over last ~6000 years, using a core from the Alfonso Basin, southern Gulf of California. They identified a period of northerly mean ITCZ position, increased monsoonal precipitation, and low productivity conditions from ~6200 to 2400 yr BP, followed by dry, productive conditions from ~2400 to 1900 yr BP. A cold dry period from 700 to 500 yr BP was associated with more southerly ITCZ position (Perez-Cruz, 2013). Because the Alfonso Basin is an oceanographically isolated basin located on the less productive western side (Barron et al., 2005) near the mouth of the Gulf, it is valuable to strengthen and validate these results by comparing with the high-resolution record from the more productive Guaymas Basin (this study).

Here we present a high-resolution multi-proxy paleoclimate record spanning Mid- to Late-Holocene climate variability in the Guaymas Basin, and interpret changes in the oceanographic and climate systems of the Gulf. Although uncertainty in our age model precludes confident high-resolution correlation to events in the ETNP and Mexican Highlands, approximate comparison to a record of δ^{15}N from the Peru Margin (Agnihotri et al., 2008)

2

suggests records from the Guaymas Basin and ETNP may be related.

Furthermore, records of continental aridity and Maya civilization events (Haug et al., 2003; Lachniet et al., 2017) are consistent with the climate history interpreted from the Guaymas Basin (this study). The primary datasets comprising this record are radiocarbon, lamination counting, nitrogen and carbon stable isotopes, carbon-to-nitrogen ratios, weight percent nitrogen, XRF trace metal counts, and smear slide analyses. Carbon stable isotope values and TOC:TN values rule out significant contribution of terrestrial organic matter (TOM) to the core, and nitrogen stable isotopes reflect the intensity of denitrification in the Gulf of California and may carry implications for the oceanographically connected ETNP (Altabet et al., 1995; Pride et al., 1999; Deutsch et al., 2014). Stable isotope measurements are linked to oceanographic system processes through work on modern biogeochemical cycling, biological productivity, and sedimentation in the Gulf of California.

2. Background

2.1 Oceanographic Setting

The Guaymas Basin is a silled basin located in the Central Gulf of California, with a seasonal upwelling regime and high siliceous productivity (Fig. 1). Above the sill depth of ~1500m, Guaymas Basin exchanges waters freely

with the ETNP (Thunell et al., 1993). A well-developed OMZ is present in the Guaymas Basin between ~500m and ~1000m depth, allowing for excellent preservation of organic sediments with minimal diagenesis (Altabet, 2005).

The canonical understanding of atmospheric circulation in the Gulf of California is that strong NW winter winds reverse direction to blow from the SE during the summer monsoon season (Badan-Dangon, 1991). However, Pares-Sierra et al. (2003) used satellite-derived scatterometer data to conclude that consistent SE winds are seldom observed at the sea surface, and atmospheric circulation at sea level is dominated by strong NW winds in the winter, and weak, variable, mostly NW to W winds in the summer (Fig. S1). In the modern Guaymas Basin, the seasonal northward displacement of the ITCZ during boreal summer is the cause of observed weak winds at the sea surface in the Central Gulf of California, which result in decreased wind-driven upwelling and a warm stratified sea surface (Pares-Sierra et al., 2003). Meanwhile, southerly summer winds in Northern Mexico and the southwest United States mark the onset of the North American Monsoon (NAM) and bring associated increases in thunderstorms and precipitation. Pares-Sierra et al. (2003) suggest that the monsoonal reversing winds paradigm originated from very few observations at coastal stations and extrapolation from high-altitude wind regimes (which do exhibit seasonal reversal), and that weak seasonal wind reversal is only observed in the southernmost part of the Gulf of California. Although seasonal reversal has been exaggerated, the strong NW winds of the winter season have

4

an important effect on productivity and nutrient cycling at the study cite in the Guaymas Basin: NW winds create offshore Ekman transport along the eastern side of the Gulf, stimulating nutrient rich upwelling, and peak biosiliceous productivity during fall and winter (Pichevin et al., 2012).

2.2 Geological Setting

The Gulf of California lies on an active divergent plate boundary between the North American and Pacific plates. The Baja Peninsula forms the western boundary of the Gulf, and is separating from the mainland at a rate of ~6cm/year, moving along en echelon set of spreading centers and perpendicular transform faults (Larson, 1972). The Guaymas Basin is one of several geologically active basins opened by this spreading; it contains hydrothermal vents, basaltic sills intruding the sediment pile, and two ~1900m deep troughs formed by active spreading segments. The high accumulation rate of low-density siliceous sediment and active geological setting lead to mass wasting events and turbidity flows which transport sediment downslope, eventually depositing turbidites in the two deep troughs (Einsele et al., 1982). Seismic profiling studies show evidence of slumping, low-angle erosion surfaces, and soft sediment deformation (Fig. S2) near the Core P12 study site (Moore, 1973). Einsele et al. (1982) analyzed the sedimentology and lithology of turbidite

deposits in the Guaymas Basin, and estimated that ~28% of turbidite sediment was eroded from locations on the continental shelves. The frequency of turbidite erosion events in the Guaymas Basin is much higher than elsewhere in the Gulf, roughly estimated to be a minimum of one event per ~2000 years (Einsele et al., 1982).

Thunell (1998) used a six-year time series of sediment trap samples to describe particle flux in the Guaymas Basin in detail. Modern sediment flux in the Guaymas basin consists primarily of three components: siliceous biogenic material (diatoms), terrigenous sediment, and calcium carbonate (Thunell, 1998). Baumgartner et al. (1991) compared a continuous record of mass accumulation rate in the Guaymas Basin to river discharge data from 1934-1966, which resolves the construction of dams on the major Sonoran rivers in the 1940's. No relationship was observed between the dam-controlled discharge of Sonoran rivers and mass accumulation rate in the Guaymas Basin, and only a weak relationship between "free, undammed" river discharge and mass accumulation of sediment was found. Because variations in river discharge do not appreciably affect the accumulation of sediment, it was concluded that terrigenous material in the Guaymas Basin is eolian in source (Baumgartner et al., 1991). Major eolian transport of dust is commonly associated with convective thunderstorms in the Sonoran Desert, which occur seasonally between July and September (Pewe et al., 1981; Brazel and Hsu, 1981). Siliceous and eolian particle flux varies seasonally in the Guaymas Basin, causing

deposition of annual varved couplets: light-colored laminations are formed during the winter upwelling season when siliceous biogenic material dominates particle flux, and dark-colored laminations result from higher relative eolian input during the stormy and relatively stratified summer conditions (Thunell, 1998). Calcium carbonate flux can vary by an order of magnitude seasonally and inter-annually and can account for up to 20% of sediment flux at times (Thunell, 1998).

In a paleoclimate context, eolian transport is often considered a proxy for aridity of the source region, however this paradigm may be oversimplified for the Sonoran Desert due to overall high aridity in the region, and the importance of convective thunderstorms in transport of eolian material. Brazel and Hsu (1981) used precipitation data from the Northern Sonaran Desert in Arizona to show that even with convective thunderstorms, it is rare for the soil in the Sonaran Desert to be moist enough during summer to prevent eolian transport of sediment. Baumgartner et al. (1991) suggest that because eolian dust transport occurs via a mechanism of convective thunderstorms, increased eolian transport may actually be associated with *increased* summer precipitation in the Sonoran Desert. Brazel and Nickling (1986), however, point out that winter precipitation provides the overriding control on eolian particle entrainment in the Sonoran Desert by controlling vegetative growth and biological soil crusting. Eolian sediment accumulation in the Guaymas Basin is a result of the interplay of complex climate processes, and may be positively related to either increased

summer thunderstorm frequency and intensity or increased aridity in the Sonoran Desert.

2.3 Oxygen Minimum Zones and Denitrification

The Guaymas Basin combines oceanographic connectivity to the ETNP (Lavin and Marinone, 2003) with high productivity, high sedimentation rates, a strong seasonal upwelling regime, and a well-developed OMZ, making it an ideal sedimentary recorder of paleoclimate conditions in the region. Measurements of the water column in the Guaymas Basin show the modern $\delta^{15}N$ of NO_3- to be ~12‰ (Pride et al., 1999). N-fixation introduces NO_3- of ~ -1‰ to the system (Brandes and Devol, 2002), while denitrification causes an enrichment of the remaining NO_3- pool to ~25‰ (Sigman et al., 2009). Because primary producers in the Guaymas Basin utilize the NO_3- pool in the water column and are the main contributor to export flux, the $\delta^{15}N$ of bulk sediment faithfully records changes in $\delta^{15}N$ of the water column NO_3- pool (Altabet, 2005). Post-depositional diagenetic alteration of $\delta^{15}N$ is usually unimportant in settings like the Guaymas Basin that show high export-flux, low oxygen, and excellent organic matter preservation (Altabet, 2005).

Denitrification, the microbially-mediated process of NO_3- reduction to N_2, is important in regulating bio-available Nitrogen in the global ocean. Since Nitrogen is a common limiting nutrient, changes in denitrification can have

significant effects on primary productivity and therefore atmospheric CO_2 concentrations and climate. The vast majority of global water-column denitrification occurs within the ETNP OMZ, making this region an incredibly important component of the global ocean-atmosphere-climate system (Deutsch et al., 2001; Altabet et al., 1995). Today, the ETNP hosts the largest pool of suboxic (<4.5 μmol kg^{-1} dissolved oxygen) waters in the ocean (Karstensen et al., 2008). Most climate models predict that OMZs will expand with climate warming (Bopp et al., 2002), which is consistent with paleoceanographic work by Liu et al. (2005, 2008) showing that the ETNP OMZ extent expanded and denitrification increased during past interglacial warm periods. However, climate models of denitrification in the ETNP have high uncertainty (Bopp et al., 2013), so high resolution records of past denitrification are important for improving predictions of the effects of anthropogenic climate change on ETNP N and N_2O dynamics. Although a strong teleconnection between the Guaymas Basin and ETNP is not established, the Guaymas Basin does receive water advected from the ETNP (Lavin and Marinone, 2003), so it is inferred that the paleoclimate signals recorded in the Guaymas Basin may in part follow changes in conditions in the ETNP.

2.4 Relevant Paleoceanographic Findings

Pride et al. (1999) used $\delta^{15}N$, opal content, and opal accumulation rates to investigate global climate change response in the Central Gulf of California on glacial-interglacial time scales. At the end of the last glacial maximum, during the Younger-Dryas, and in the middle to late Holocene, Pride et al. (1999) observed homogenous sediments with low $\delta^{15}N_{org}$ and low opal content. During deglacial stages laminated sediments with high $\delta^{15}N_{org}$ and high opal content were observed. These major glacial-deglacial changes were interpreted to reflect significant and widespread changes in the extent of the ETNP OMZ, and thus rates of denitrification. The record interpreted in this study does not span a glacial-deglacial transition, however it is useful to consider the ~2800 year record from Core P12 within the context of glacial-interglacial changes.

Perez-Cruz (2013) used trace metal records generated from core T34 in the Alfonso Basin, a marginal basin in the Southern Gulf of California, to investigate changes in precipitation associated with ITCZ migration over the last ~6000 years. The Alfonso Basin is unique in the Gulf of California for its relatively restricted communication with Pacific waters (sill depth 250m), and the significant riverine runoff it receives from flash floods in the small volcanic alumino-silicate rich drainages surrounding the basin, which allow changes in riverine input to be interpreted form records of Al, Ba, Ca, Fe, Si, Ti, and Zr (Perez-Cruz, 2013). Perez-Cruz (2013) identified a period of increased

precipitation from 6200 to 2400 yr BP, a drought from 2400 to 1900 yr BP, and a cold dry period characterized by strong eolian input and high productivity from 1900 to 300 yr BP. Dry productive conditions are linked to a southerly ITCZ, and wet conditions to a more northerly ITCZ position (Perez-Cruz, 2013).

Barron et al. (2004) produce a relatively high-resolution 15,000-year paleoclimate record of microfossil assemblages, biogenic silica, and $CaCO_3$ in the Guaymas Basin. Barron et al. (2004) characterize the Bolling-Allerod (14,600 to 12,900 yr BP) as a high biogenic silica, low $CaCO_3$ deposition regime, similar to modern conditions in the Guaymas Basin and the Younger-Dryas (12,900 to 11,600 yr BP) as a less productive interval with weaker upwelling and a higher proportion of $CaCO_3$. Increased abundances of *O. pulchra* and *R. tesselata* (an upwelling associated silicoflagellate, and diatom, respectively) are interpreted in conjunction with decreased $CaCO_3$ and higher amplitudes of variance in terrigenous proxies to reflect enhanced spring upwelling, possible intensification of ENSO, and the beginning of modern high-productivity conditions in the Guaymas Basin after 2800 yr BP.

3. Materials and Methods

3.1 Core Description

      Core P12 was lifted from 667m water depth on the North flank of the Guaymas Basin, near the eastern margin of the Central Gulf of California at 27° 52.1129' N by 111° 41.5062' W (Fig. 1).   The core is 394.5cm long, and shows well-preserved mm-scale lamination in the upper 294.5cm due to the inhibition of biotrubation by anoxic conditions at the core site. The bottom ~95cm are heavily bioturbated and massive, indicating a period of oxygenated conditions at the study area; this study will focus on the mm-scale laminated upper 294.5cm, referred to hereafter as the "Core P12 record".

3.2 Dating Methods

      3.2.1 Radiocarbon Dating

      23 samples were analyzed for radiocarbon: 8 from Core P12, and 15 from 6 other Guaymas Basin cores. Each sample integrates across 1 cm depth in the core. Samples were freeze-dried, homogenized, and acidified to remove $CaCO_3$, allowing for the analysis of remaining organic matter.   Acidification was performed on ~200mg of sample, which was treated with ~5ml buffered pH 5

acetic acid solution for ~24 hours to dissolve the CaCO$_3$. Samples were then

rinsed with Milli-Q water 6 to 8 times to remove the acetic acid. Acidified

samples were then freeze-dried again, re-homogenized and stored for ^{14}C and

^{13}C analysis. Radiocarbon dating was performed at Lawrence Livermore

National Laboratory Center for Accelerator Mass Spectrometry. Methods

followed Center for Accelerator Mass Spectrometry standard operating

procedures for sediment samples.

The resulting ^{14}C ages were corrected using the Calib 7.1 Marine13

calibration curve and a Delta-R of 406 +/- 121 calendar years, calculated from

the mean of the twelve bivalve measurements in the Marine Reservoir

Correction Database (http://calib.qub.ac.uk/marine/) located nearest the study

site.

9 samples spanning the Core P12 record were washed and sieved into

>63um, and <63um fractions. Both size fractions, as well as the fines that passed

through the sieves were inspected for charcoal fragments or fines, hydrocarbon

residue, or other foreign organic matter.

3.2.2 Layer Counting

Visual layer counting was performed on high-resolution core images.

Image editing software was used to mark the center of the light-colored lamina

in each light-dark couplet. The location coordinates of each mark on a light-

colored lamina were then exported to data-processing software and converted

to depth in core (Fig. 4). The resulting data set lists the depth of each discernible

light-colored lamina in the core, and constrains the total number of lamina that

comprise the Core P12 record.

3.3 Isotopic and Elemental Analysis

Carbon and nitrogen isotopic and elemental composition was determined

at the Stable Isotope Laboratory (SIL) at University of California, Santa Cruz

(UCSC). Bulk sediment $\delta^{15}N$ and elemental ratio data were collected using 20mg

samples in Sn capsules; organic $\delta^{13}C$ and elemental composition data were

collected using 2.5mg samples of acidified sediment in Sn capsules. All samples

were measured by Dumas combustion performed on a Carlo Erba 1108

elemental analyzer coupled to a ThermoFinnigan Delt Plus XP isotope ratio mass

spectrometer (EA-IRMS). An in-house gelatin standard, Acetanilide, and an in-

house bulk sediment standard, "Monterey Bay Sediment Standard", were used in

all runs. Reproducibility of an in-house matrix-matched sediment standard is

<0.1‰ VPDB for $\delta^{13}C$ and <0.2‰ AIR for $\delta^{15}N$. Data is corrected for blank, and

for drift when appropriate. Carbon and nitrogen elemental composition was

estimated based on standards of known composition, for which analytical

precision is determined to be better than 1 %.

3.4 X-Ray Flourescence (XRF) Scanning

X-Ray Flourescence (XRF) scanning was performed on an Avaatech XRF core-scanner at Scripps Institute of Oceanography. A 12mm cross-core swath was scanned with 2mm downcore slit size at 2mm down-core resolution spacing. Three scans were performed at 10kV 500uA (no filter), 30kV 2000uA (thick Pd filter), and 50kV 2000uA (Cu filter), providing high-resolution, non-destructive analysis of elements from Al to Ba. Due to the mechanism used to mount the core on the XRF core-scanner, the core was scanned in 3 separate ~1m long sections. Because of this mechanism, ~4cm at the ends of each core section cannot be scanned, so small amounts of the XRF record are missing at each core section break.

3.5 Smear Slides

Smear slide analysis was performed on 16 samples, using 3 randomized counts per sample. Percent cover of major constituents was visually estimated following the method described by Drake et al. (2014). Intervals with particularly high or low Ca:Ti ratios were selected for smear slide analysis, in order to determine the cause of variability in the Ca:Ti record (Fig. S7). Light and dark lamina were also separately sampled and analyzed in order to investigate lithological differences within couplets.

4. Results

4.1 Age Model / Chronology

8 radiocarbon measurements in the laminated section of core P12 provide absolute chronology for the core. Linear extrapolation between these 8 radiocarbon dates yields a coretop age of ~1300 yr BP, and an age of 4087 yr BP at 294.5 cm depth, indicating that the Core P12 record spans ~2800 years. Bomb radiocarbon is not observed at the shallowest radiocarbon sample (5.5cm). Visual layer counting of annual varves documented only 1566 annual couplets in the same 294.5 cm interval dated by radiocarbon. Thus varve counting suggests that the Core P12 record represents only 1566 years of sediment accumulation, about 1200 years less than indicated by radiocarbon dating (Fig. 2). Error in radiocarbon dating was quantified using 1-σ probability distributions, which range from +/-129 years to +/-174 years with a mean 1-σ distribution of +/-153 years. Visual inspection revealed one probable angular unconformity or erosion surface at 256.5cm depth. No charcoal, soil organic matter, or any other foreign organic matter was detected in any size fraction of the 9 samples washed.

4.2 Stable Isotopes and Elemental Composition

Many of the Core P12 stable isotope and elemental composition records show clear differences between the segments above versus below 100cm depth,

16

or 2800 yr BP age (Fig. 3). This observation is consistent with the work of Barron et al. (2004), who observed increased numbers of *O. Pulchra* and increased amplitude of terrigenous input proxies after 2800 yr BP in the nearby DSDP hole 480. Because of the clear changes observed at 2800 yr BP in the Core P12 record, and its consistency with previous work, we choose to divide the measured paleoproxy records at 2800 yr BP and focus our analysis on comparing the older section to the younger.

Mean bulk sediment carbon-to-nitrogen ratios (TC:TN) are significantly ($p < 0.0001$) lower after 2800 yr BP (9.10) than prior to 2800 yr BP (9.77).

Organic carbon-to-nitrogen ratios (TOC:TN) are also significantly lower after 2800 yr BP, although the difference is smaller than the difference in TC:TN. Mean TOC:TN before 2800 yr BP is 8.56, and mean TOC:TN is 8.35 after 2800 yr BP ($p < 0.0013$).

$\delta^{13}C$ ranges from -22.10‰ to -20.13‰, with mean -20.69‰, and standard deviation 0.27‰ (Fig. S3). Mean $\delta^{13}C$ is -20.62‰ before 2800 yr BP, and -20.74‰ after 2800 yr BP ($p < 0.0494$). The correlation coefficient between $\delta^{13}C$ and C:N organic is -0.04.

Mean bulk $\delta^{15}N$ is 11.15‰ prior to 2800 yr BP. After 2800 yr BP mean bulk $\delta^{15}N$ is 10.52‰, or 0.63‰ lower ($p < 0.0001$). $\delta^{15}N$ shows a strong positive correlation with TC:TN (R=0.41), but Ca:Ti and $\delta^{15}N$ are not correlated (R=-0.11). Refer to Supplementary Material section 1.1 and Supplementary Figure 4 (Fig. S4) for a discussion of corrections applied to $\delta^{15}N$ data.

Mean bulk weight percent Nitrogen is 0.37% before 2800 yr BP, and
0.41% after 2800 yr BP (p < 0.0001). The standard deviation of wt% Nitrogen
throughout the core is 0.03%. Mean organic weight percent Nitrogen is also
higher after 2800 yr BP: it is 0.51% prior to 2800 yr BP and 0.59% after 2800 yr
BP (p < 0.0203). The standard deviation of mean organic weight percent
Nitrogen throughout the core is 0.16%.

4.3 Ca:Ti Ratio and PCA of other XRF Core Scan Data

Mean Ca:Ti ratio is 1.76 in before 2800 yr BP and 2.68 after 2800 yr BP(P
< 0.0001). The standard deviation Ca:Ti ratio throughout the core is 1.57.

Principle component analysis of the XRF core scan data revealed 4 main
principle components (PCs) that account for 54% of the total variability in XRF
data (principle components 1-4 represent 33%, 9%, 7%, and 5%, respectively).
PC 1 is strongly related to the detrital elements (K, Fe, Ti, Al, and Sr) and lacks a
strong relationship to the water-content elements (Br, Cl, and S) (Fig. 5). PCs 2,
3, and 4 show strong relationships with the water-content related elements Br,
Cl, and S and weak relationships with detrital (K, Fe, Ti, Al, Sr) elements (Fig. S8).
PC 1, which accounts for 33% of the variance in the XRF core scan data, changes
significantly at 2800 yr BP: PC 1 has a mean z-score of 0.52 before 2800 yr BP,
and a lower z-score of -0.71 after 2800 yr BP (p<0.0001).

4.4 Smear Slide Analysis

A low-resolution smear slide analysis was performed for two reasons: to characterize the lithology of light and dark laminae, and to calibrate the Ca: Ti record by documenting lithological differences between intervals of high vs. low Ca:Ti. Analysis of 16 samples with 3 separate counts per sample showed high percent cover coccolithophores to coincide with high Ca:Ti (Fig. 6). Conversely, few to no coccolithophores were observed in intervals with low Ca:Ti. Both percent cover of coccoliths and Ca:Ti are higher in the older part of the core. Smear slide analysis revealed no obvious dilution of the coccolith signal by changes in the relative amount of eolian terrigenous material.

Smear slide counts show that percent cover pennate diatoms varies strongly between light and dark laminations: light laminae average 45% cover and dark laminae average 26% cover ($p < 0.0001$). Terrigenous materials (clay and siliciclastics) also show a significant ($p < 0.0031$) difference between light and dark laminae: light laminae average 7% cover and dark laminae average 13% cover. Although the smear slide analysis is not very high resolution, it is sufficient to characterize the composition of light and dark laminae and to calibrate the Ca:Ti record.

5. Discussion

5.1 Chronology

Comparison of layer counting chronology and radiocarbon dating reveals two unusual results. First, radiocarbon provides absolute chronology, dating the coretop to ~1300 yr BP. Second, layer counting suggests that the Core P12 record (0-294.5cm) represents only ~1600 years of deposition, whereas the 8 radiocarbon dates in the same interval span ~2800 years. There are two possible mechanisms that could cause layer counting and radiocarbon dating methods to yield different results. The first possibility is that varve chronology represents the true age of the core, and radiocarbon in the sediment is affected by factors other than age. For example, changes in upwelling, input of "old" radiocarbon from a source such as hydrocarbons, hydrothermal vent seeps, charcoal, or terrestrial organic matter (TOM) could alter the $\delta^{14}C$ values of organic matter in Core P12. DeMaster and Turekian (1987) encountered similar disagreement between radiocarbon and varve-counting chronologies in the Carmen Basin, Gulf of California, and invoked a monotonic decrease in upwelling intensity to explain the discrepancy. The second possibility is that the radiocarbon dates reflect the true age of the sediment, and the varved record is not continuous throughout the core: ~1200 annual varves may be "missing" from the record due to erosion, mass wasting events, or soft sediment

20

deformation. Alternatively, annual deposition across the Guaymas Basin may be spatially patchy, so the Core P12 site may not receive a full light-dark couplet every year. Hendy et al. (2013) compared radiocarbon dates from marine organic matter and terrestrial charcoal within a Santa Barbara Basin core to constrain changes in reservoir age and sedimentation. They determined that a ~150 year change in reservoir age (from 350 to 500 years) explained a portion of the difference between dating techniques, but could not explain the full discrepancy. In addition to a small change in upwelling 1 out of every ~3.3 varves were shown to be missing from the sedimentary record due to erosion or patchy deposition. It is extremely difficult to constrain exactly how much erosion and how much change in upwelling/change in reservoir age explains the differences in core P12 without very high-resolution radiocarbon dating and independent charcoal dates after Hendy et al. (2013). However, radiocarbon, smear slide, observations of washed samples, and comparison to other sites in the Guaymas Basin, suggest that the P12 coretop is 1300 years old, and that the discrepancy between varve-counting and radiocarbon in Core P12 cannot be reasonably explained by changes in upwelling or addition of old carbon. Therefore, erosion of some laminae, or non-annual deposition at the P12 site must explain all or most of the ~1200 year discrepancy between dating methods. We adopt a linear interpolation of the 8 radiocarbon dates as the most accurate possible Core P12 age model, given the available data.

A core missing ~1300 years, or roughly ~2.6m of sediment, from the coretop is an unusual finding in a high-productivity, high-sedimentation setting like the Guaymas Basin. However, close scrutiny of the radiocarbon data, and comparison to other sites in the Guaymas Basin suggest that error, changes in upwelling intensity, and addition of foreign organic matter cannot explain the coretop age. Error in the radiocarbon dates is an order of magnitude too small to explain the 1300-year old coretop. Furthermore, bomb radiocarbon is expected in samples from modern coretops, but is not observed at the shallowest measured radiocarbon sample in Core P12 (5.5cm). The average couplet thickness in the core is ~2mm, so if couplets were annual and the sedimentary record was complete, sediment at 5.5cm should be ~ 27 years old, and should contain bomb radiocarbon from the 1963 "bomb-spike". The absence of bomb radiocarbon at 5.5cm suggests that the measured sample cannot be modern. Also, changes in intensity of upwelling of "old" deep water cannot explain the observed Δ14C measurements in core P12. Pearson et al. (2005) measured the Δ14C of bottom water in the Guaymas Basin to be -228 +/- 6‰. But the shallowest measured sample in P12 (5.5cm) shows a Δ14C of -239.1‰, an isotopic signature that cannot be produced by the addition of any amount of upwelled -228‰ deep water. The mean Δ14C of twelve nearby bivalve shells collected before bomb testing show that pre-bomb surface water in the Guaymas Basin was ~ -102‰: again no amount of upwelled -102‰ water can create a coretop Δ14C of -239‰. This rules out the possibility that

the coretop is pre-bomb in age, but much younger than 1300 yr BP. Finally,

although the Guaymas Basin contains hydrothermal seeps, hydrocarbons, and

methanogenic bacterial mats that produce "radiocarbon dead" organic matter of

$\sim$ -930‰ (Pearson et al., 2005), these sources are unlikely to affect core P12.

No bacterial mats, hydrothermal seeps, or hydrocarbons are observed near site

P12. Furthermore, we measured radiocarbon from two Guaymas Basin cores

collected in deeper water proximal to vent sites (cores P10 and P11), which

showed less negative Δ14C coretop values and younger coretop ages (-157.2‰

at 1.5cm depth, and -180‰ at 3.5cm depth, respectively). This spatial pattern

suggests that the unusually negative Δ14C coretop values and old coretop age of

Core P12 cannot be due to the incorporation of radiocarbon from vent

hydrocarbons or bacterial mats.   If the Guaymas Basin vent systems were a

significant source of old radiocarbon to the sediment, measurements of coretops

proximal to vent sites should yield more negative coretop Δ14C values, and

older coretop radiocarbon ages than sites distal from vents such as Core P12.

The second unusual observation in Core P12 is the downcore-increasing

discrepancy between radiocarbon and layer counting chronologies, which

culminates in a maximum difference of $\sim$1200 years at the bottom of the core

(294.5cm). $\delta^{13}C$ and TC:TN values indicate a strong marine organic matter

signature, suggesting that terrestrial organic matter, charcoal, or soils do not

make a significant contribution to the organic matter at site P12. Furthermore,

no charcoal, soil organic matter, or other potential sources of "old" radiocarbon

were observed in smearslides or any size-fraction of the washed and sieved samples. Changes in reservoir age or upwelling intensity are cannot explain this discrepancy either: if a large monotonic decrease in upwelling occurred in the Guaymas Basin, significant trends in paleoproductivity, couplet thickness, $\delta^{13}C$, and other paleo-proxies would be expected. No trends consistent with a large decrease in upwelling are observed in any of the measured paleo-proxy records.

Finally, although the available data does not conclusively prove that erosion or incomplete deposition are the cause of the 1300 year old coretop age and ~1200 year discrepancy between dating techniques, this mechanism is the most likely explanation and is consistent with the geological setting in the Guaymas Basin. It is well established that light-dark couplets in the Guaymas Basin represent annual varves, with light-colored diatom-rich layers deposited during the highly productive winter upwelling season, and dark layers with a higher proportion of eolian material deposited during the stratified summer season (Baumgartner et al., 1985; Thunell et al., 1993). However, geological processes could cause individual laminae or groups of laminations to be absent from the sedimentary record. These mechanisms can be divided into two categories: geological mechanisms for erosion, and processes that cause laminations not to be deposited in the first place. Mechanisms for erosion are numerous (mass-wasting events, scouring erosion by turbidity currents, soft sediment deformation, slumping, etc.) and occur easily in low-density unconsolidated sediments. Because numerous turbidite sequences are observed

in at the bottom of the Guaymas Basin, and it is estimated that at least 28% of the turbidite sediment originates on the continental shelf within 30-80km of the turbidite deposition area (Einsele et al., 1982), it is possible that sediment from Core P12 has been removed by the erosive action of turbidity currents. There are also processes that cause patchy to irregular deposition of marine sediments. It is possible that during the Mid- to Late Holocene not every winter upwelling season produced a significant diatom bloom in the Guaymas Basin. Even if a diatom bloom was produced every season, mesoscale-eddies, bottom currents, and grazing by zooplankton could prevent some blooms from evenly blanketing the entire seafloor. Similarly, a particularly moist or calm summer season could inhibit the seasonal deposition of the dark eolian layer that defines the boundary between two annual diatom blooms. Missing one or several dark eolian lamina could bias varve chronology by making several annual diatomaceous layers appear as one thick layer.

In summary, the Core P12 study site must be missing ~1300 varves from the coretop, and another ~1200 varves throughout the core, due to erosion or patchy to irregular deposition. Because no bomb radiocarbon is measured, no vent/hydrocarbon effects on radiocarbon are observed, no evidence of terrestrial organic matter is measured, and the Δ14C of Guaymas bottom water is not negative enough to create the Δ14C values measured from core P12, erosion or patchy deposition of varves must have caused a ~1300-year-old coretop and downcore divergence between radiocarbon and varve-chronology

age models. Therefore the age model adopted here is a linear interpolation in age-depth space between the 8 radiocarbon dates. This is an important result, as it shows that despite well-documented annual varve formation (Thunell et al., 1993), layer counting is not likely a reliable dating method in this setting.

5.2 Change in Community Composition at ~ 2800 yr BP

Records of Ca:Ti, TOC:TN, TC:TN, weight percent nitrogen, and PC 1 from Core P12 all differ significantly after 2800 yr BP compared to before 2800 yr BP (section 4.2). Before interpreting these changes to reflect paleoceanographic conditions, the influence of TOM must be ruled out. Typical terrigenous TC:TN values range from 20 to 200 (Hedges et al, 1986; Emerson and Hedges, 1988). Silverberg et al. (2014) reported TOC:TN of POC in the Alfonso Basin, Gulf of California, to range between 5.7 and 11.6 with a mean of 8.9, and Thunell (1998) measured TOC:TN of marine organic matter from sediment traps in the Gulf of California ranging from 5 to 10.5 with over 85% of TOC:TN ratios between 5.0 and 8.0. Observed mean TOC:TN in Core P12 is 8.4, with a range of 7.2 to 9.8. The mean TC:TN measured in Core P12 is 9.5, with a range of 8.7 to 11.2, and standard deviation 0.5. The measured carbon-to-nitrogen from Core P12 fall within the range of classic marine TOC:TN ratios, a result which is consistent with the δ^{13}C values in suggesting that the contribution of TOM to this core is minimal. Because TOM is minimal to absent in Core P12, the statistically

significant difference in Ca:Ti, TOC:TN, TC:TN, weight percent nitrogen, and PC 1

before 2800 yr BP compared to after 2800 yr BP can be interpreted in

conjunction with smear slide analysis results to indicate lower relative

contribution of coccolith microfossils after ~2800 yr BP.

Mean Ca:Ti is much lower ($p<0.0001$) after 2800 yr BP (1.76) than before

2800 yr BP (2.68). Because of the positive relationship observed between the

relative percent cover coccoliths and Ca:Ti (See Section 4.4, Fig. 6), the Ca:Ti

record can be interpreted as a proxy for relative contribution of coccoliths to the

sediment. Ti is supplied to the Guaymas Basin from a terrigenous source via

eolian transport during summer storms in the Sonoran Desert, whereas Ca can

be supplied either by a terrigenous source, or by calcareous plankton.

Interpreting Ca:Ti as a proxy for relative contribution of coccoliths to the

sediment suggests that oceanographic conditions in the Guaymas Basin changed

around 2800 yr BP: mean conditions must have shifted from stratified low-

nutrient conditions that favor coccolithophore productivity prior to 2800 yr BP

to a regime characterized by stronger seasonal winds, increased upwelling, and

stronger dominance of diatom productivity over coccolithophores after 2800 yr

BP.

The observed change in TOC:TN ratios from a mean of 8.56 before 2800

yr BP to 8.35 after 2800 yr BP ($p<0.0013$) can also be explained by a change in

the relative contribution of coccoliths to the sediment. Brzezinski (1985)

measured diatoms in culture, and established the canonical TOC:TN ratio of 8.1

for diatom organic matter. Engel et al. (2014) cultured the coccolithophore *Emiliana Huxleyi* and measured DOC:DON ratios from 8.4-8.6 and POC:PN ratios from 16.6-17.2. The observed decreased in mean TOC:TN at 2800 yr BP reflects decreased relative contribution of coccoliths (high TOC:TN values) and corresponding increase in diatom productivity (lower TOC:TN values) at 2800 yr BP. Again, this change in community composition most likely reflects a change in oceanographic conditions in the Guaymas Basin at 2800 yr BP.

Mean TC:TN is also lower (p<0.0001) after 2800 yr BP (9.10) than before 2800 yr BP (9.77). Coccolithophores contribute carbon to the sediment in two different ways: organic carbon, and $CaCO_3$ microfossils (coccoliths). The effect of coccolithophore organic carbon on the TOC:TN record is described above, and the corresponding contribution of $CaCO_3$ from coccoliths likely drives the observed change in the TC:TN record. Therefore, the lower observed TC:TN after 2800 yr BP is likely also a result of decreased coccolith contribution to the sediment. Ca:Ti is strongly correlated to TC:TN (R=0.66), and also exhibits tight coupling of short term variability, because both signals reflect variations in percent coccoliths (Fig. 6).

The higher values of weight percent nitrogen observed after 2800 yr BP (0.41%) compared to before 2800 yr BP (0.37%) are also consistent with a change in productivity. The difference is not likely to be caused by a diagenetic artifact, since anoxic conditions persistent at the study site minimize microbial nitrogen remineralization, (Robinson et al., 2012).

Principle Component 1 (PC 1) is interpreted as a proxy for the relative

contribution of eolian material to the sediment because of its strong relationship

to the detrital-source elements (K, Fe, Ti, Al, and Sr), and shows a significantly

(p<0.0001) lower z-score after 2800 yr BP (-0.71) than before 2800 yr BP (0.52).

This result suggests that on average, the half of the record prior to 2800 yr BP

contains a higher relative proportion of eolian material. It is possible that this

signal reflects a change in convective thunderstorm intensity, continental aridity

and absolute eolian flux. However, considering the other stable isotope and

elemental composition records presented here, a more likely explanation is that

the significantly lower PC 1 z-score after 2800 yr BP reflects more dilution of

eolian material by a much higher flux of siliceous productivity.

In summary, records of Ca:Ti, TOC:TN, TC:TN, weight percent nitrogen,

and PC 1 all differ significantly after 2800 yr BP compared to before 2800 yr BP,

a change which can be interpreted to reflect the relative contribution of

coccoliths to the sediment. In the Gulf of California, coccolithophore fluxes are

highest during periods of low nutrient concentrations and strong stratification,

which occur in the modern Gulf seasonally during summer and fall when the

ITCZ is at its northernmost position (Thunell, 1998). The lower contribution of

coccoliths to Core P12 after 2800 yr BP indicates a shift in mean conditions from

more stratified, nutrient-poor surface waters prior to 2800 yr BP to more

nutrient-rich conditions with stronger upwelling and higher rates of siliceous

productivity after 2800 yr BP (Fig. 7). In other words, mean conditions in the

Gulf prior to 2800 yr BP were more similar to modern summer conditions, characterized by weak winds (Pares-Sierra et al., 2003), low siliceous productivity (Thunell et al., 1993), and a more northerly ITCZ position in both the Pacific and Atlantic basins (Poore et al., 2004).

Several paleoceanographic records from the region support this conclusion. Barron et al. (2004) interpret a similar change at 2800 yr BP from DSDP Hole 480, located near the Core P12 site in the Guaymas Basin. Lower $CaCO_3$ and higher *O. pulchra* and *R. tesselata* abundances after 2800 yr BP are associated with stratified, nutrient-poor conditions, and interpreted to reflect enhanced upwelling, possible intensification of ENSO, and the "onset of modern oceanographic conditions" in the Guaymas Basin (Barron et al., 2004). In the Alfonso Basin, southern Gulf of California, Perez-Cruz (2013) identify a period of northward mean ITCZ position, increased monsoonal precipitation, and low productivity conditions from ~6200-2400 calendar yr BP, followed by dry, productive conditions from ~2400-1900 yr BP. The age model of Perez-Cruz (2013) is based on 6 radiocarbon dates measured on benthic foraminifera; 3 of these overlap the interval recorded in Guaymas Core P12, including a radiocarbon date at ~ 2800 yr BP. Estimates of Sedimentation rates from the Alfonso Basin are lower in the Mid-Holocene (0.27 mm/yr) and increase to 0.61 mm/yr and 0.51 mm/yr in the Late-Holocene (Perez-Cruz, 2013), which is consistent with the increased upwelling and productivity and more southerly ITCZ position after 2800 yr BP interpreted from Core P12 in the Guaymas Basin

(this study). Overall, this study corroborates the conclusion of Perez-Cruz

(2013) that the mean ITCZ position migrated southward during the Mid- to Late-

Holocene. The Alfonso Basin record does not show the relatively sharp

transition at 2800 yr BP observed in the Guaymas Basin core P12 (this study)

and nearby DSDP site 480 (Barron et al., 2004). This is not surprising, since the

Alfonso Basin is located on the western side of the Gulf ~300km south of the

Guaymas Basin, and differs oceanographically from the Guaymas Basin (semi-

enclosed basin, less upwelling, receives riverine runoff). Finally, records of

Globigerinoides sacculifer abundance from the Pigmy Basin, Gulf of Mexico also

suggest a trend of southward mean ITCZ migration from 4200 to 1300 yr BP

(Poore et al., 2004).

5.3 Denitrification and $\delta^{15}N$

Several processes can affect bulk sediment $\delta^{15}N$: incomplete utilization of

NO_3^-, diagenetic alteration, terrestrial organic matter (TOM), nitrogen-fixation,

and denitrification. The first four processes can be ruled out, or shown to be

negligible, by previous work. By process of elimination, denitrification is left as

the main process that dictates $\delta^{15}N$ in the Guaymas Basin record, so $\delta^{15}N$ can be

used as a proxy for denitrification and therefore ventilation and OMZ intensity in

the past. Each process affecting bulk $\delta^{15}N$ will be addressed in order:

1. The Guaymas basin is highly productive, with a seasonal upwelling regime, and experiences complete nutrient utilization annually (Pichevin et al., 2012).

2. Altabet et al. (1999) compare sediment trap $\delta^{15}N$, water column $\delta^{15}NO_3$-, and core top $\delta^{15}N$ bulk, concluding that diagenetic effects on bulk sediment $\delta^{15}N$ are minor in the highly productive Gulf of California. This is in agreement with Robinson et al. (2012), who reviewed over 100 measurements of $\delta^{15}N$ from sediment traps and surface sediments and found that in regions with high sedimentation rates, such as the Gulf of California, d15N of surface sediments are very similar to $\delta^{15}N$ of sinking particles. This indicates that diagenetic alteration of $\delta^{15}N$ sediment is not significant in these regions. Extensive work by Dean et al. (2004) and Kienast et al. (2002) also shows that *in situ* diagenesis does not affect $\delta^{15}N$ significantly in the highly productive basins of the Gulf of California.

A significant difference in $\delta^{15}N$ is observed between samples from the working half versus the archive half of Core P12. This difference is likely due to diagenetic alteration of labile N, however the remineralization of labile N from the deeper part of the core did not occur *in situ*, but rather during storage as a result of exposure to extreme and unusual temperature and oxygenation conditions. Despite this *ex situ* loss of labile N, it is believed that diagenesis did not have a significant effect on the isotopic composition of the sediment. Refer

to supplementary materials for a detailed discussion of N diagenesis and the correction applied to *ex-situ* altered archive half $\delta^{15}N$ data.

3. Analysis of modern sediment and core-top samples show that modern organic matter in the Guaymas Basin is marine in origin (Thunell, 1998). Furthermore, measurements of $\delta^{13}C$ from Core P12 suggest that the effect of TOM is minor to non-existent and is therefore unlikely to affect the bulk $\delta^{15}N$ record. Mean $\delta^{13}C$ in Core P12 is -20.69‰, a value that falls well within the canonical range of -18 to -22‰ for marine organic matter (Emerson and Hedges, 1988). TOM $\delta^{13}C$ values are typically much more negative than those measured in Core P12, ranging from -26 to -28 ‰ (Degens, 1969). Finally, Core P12 TOC:TN, $\delta^{15}N$ and $\delta^{13}C$ show no strong correlation with one another (R values < 0.26). Because TOM is characterized by high TOC:TN and low $\delta^{13}C$, if a significant amount of TOM was present in the core, a strong inverse correlation between C:N organic and $\delta^{13}C$ would be expected. No such inverse correlation is observed, confirming a minimal or nonexistent contribution of TOM to Core P12.

4. Although N-fixation by *Trichodesmium* and *Richeila* does occur in the Central Gulf of California during summer, N-fixation typically supports <10% of particulate carbon export at 100m depth (White et al., 2013). White et al. (2013) measured N_2 fixation rates to determined a 1.7% median contribution of N_2 fixation to C export in the Gulf of California and ETNP during summer. Because the small amount of N-fixation in the GoC occurs primarily during the less productive summer season, coinciding with minima in sediment

accumulation (Pichevin et al., 2012), it is inferred that N-fixation has little effect on the bulk sediment $\delta^{15}N$ record.

5. By process of elimination, bulk $\delta^{15}N$ can be interpreted as a proxy for denitrification. The observed statistically significant 0.63‰ decrease in $\delta^{15}N$ bulk sediment after ~ 2800 yr BP indicates less denitrification due to better ventilation and a weakener OMZ in the Guaymas Basin and ETNP after 2800 yr BP. Variance in the $\delta^{15}N$ record is likely controlled by changes in mean ITCZ position, which controls wind-driven upwelling, primary productivity, and oxygenation in the Guaymas Basin (Fig. 7).

5.4 High-Resolution XRF records and Shorter-term Variability

Hennekam and de Lange (2012) showed that XRF core scanning can incorporate significant errors due to variations in water content of the sediment and the thickness of the water film that forms between the sediment surface and a protective plastic film used during analysis. Comparison between XRF core scanning data and conventional XRF methods revealed that all elements from Al to Fe are subject to significant "false" variability due to this effect. Only Ca:Ti and Ca:K ratios are confirmed as accurate XRF core scanning results, due to the fact that Ca and Ti or K behave antipathetically, but react similarly to changes in water film thickness, which leaves their ratios unaffected by variability in water content and film thickness (Hennekam and de Lange, 2012).

To avoid false interpretations based on XRF core scan data affected by the above factors, traditional paleoceanographic elemental ratios are not interpreted for this study (i.e. Si:Ti, Br:Ti, Fe, Ti, Al). Instead, principle component analysis was performed on the full body of elemental data. Principle component 1 (PC 1) shows strong relationships with detrital elements (K, Fe, Ti, Al, and Sr) and is not strongly related to elements which reflect the water content of the sediment (Br, Cl, S), so it is interpreted as a proxy for relative terrigenous eolian flux to the Guaymas Basin, without risk of the XRF core scan errors described by Hennekam and de Lange (2012) (Fig. 5). However, because PC 1 reflects only the relative proportion of terrigenous eolian material, it is difficult to distinguish between changes in absolute input of eolian material and dilution of the eolian fraction by changes in siliceous and calcareous productivity. Principle components 2, 3, and 4 show strong relationships to the Br, Cl, and S, which reflect X-ray signal attenuation by water, and therefore cannot be interpreted as paleoenvironmental proxies.

Spectral analysis was used to investigate higher-frequency variance in Ca:Ti, and cross spectral analysis was used to compare frequencies of variance between the two high-resolution XRF records (Ca:Ti and PC 1, interpreted as proxies for relative contribution of coccoliths and eolian terrigenous material, respectively). Spectra of Ca:Ti against depth were very different that spectra against age. It is suspected that changes in sedimentation rate from the linear interpolation between the 8 radiocarbon dates biased the spectral analysis.

Therefore, a simplified age model (Fig. S9) was applied to the data for spectral

analysis. Because of missing data in the XRF record at breaks between ~1m core

sections (section 3.4), spectral analysis was performed separately on each of the

3 ~1m core sections: section 1 (1300 to ~2800 yr BP), section 2 (~2800 to

~3400 yr BP), and section 3 (~3400 to ~4100 yr BP).

Ca:Ti shows centennial variability with important peaks at ~200 year

periodicity in sections 1 and 2, ~170 year periodicity in section 3, decadal

variability with important peaks at ~100 and ~70 year periodicities only in

section 1 (1300 to ~2800 yr BP) (Fig. 8). The PC 1 record shows centennial

variability with important peaks at ~170 year periodicity in section 3, ~500 year

periodicity in section 2, and ~800 year periodicity in section 1, and decadal

variability with important peaks at ~120 and ~70 year periodicities only in

section 1 (1300 to ~2800 yr BP). Refer to Figure 8 for the percent variance of

each peak and frequency bands across which percent variance was calculated.

Cross-spectral analysis between the Ca:Ti and PC 1 records confirmed that

centennial variance is important throughout all three sections in both records,

and that decadal variance is important only in section 1. Coherency >0.8 in

frequencies of variance between Ca:Ti and PC 1 is observed only in section 3

(~3400 yr BP to ~4100 yr BP) at centennial scale variability bandwidth.

Centennial variance in Ca:Ti throughout the core is thought to reflect

centennial-scale variance in the ecosystem structure and relative contribution of

coccoliths in the Guaymas Basin, which are controlled by the degree of water

column stratification, wind-strength, and ITCZ position. In sections 1 and 2, where centennial-scale variance is not coherent between Ca:Ti and PC 1, Ca:Ti variance reflects relative coccolith flux to the sediment, whereas PC 1 reflects relative eolian flux. In section 3, where coherency >0.8 is observed between Ca:Ti and PC 1, the same mechanism must control both records. Because section 3 also shows the largest amplitude of variance in the relative contribution of coccoliths, it is interpreted that coccolith contribution controls both Ca:Ti and PC 1 signals during this time period. The mechanism of this control is thought to be dilution by changes in siliceous productivity: during periods of strong stratification, low nutrient conditions arise, which favor the growth of coccoliths over diatoms. Since diatoms make up the bulk of export-production in the Guaymas Basin (Thunell, 1998), an increase in coccolith productivity and reduction in diatom productivity under stratified conditions causes decreased dilution of the background eolian input, resulting in coincident centennially-paced maxima in Ca:Ti (relative coccolith flux) and PC 1 (relative eolian flux). This relationship breaks down after ~3400 yr BP, because the amplitude in Ca:Ti variance decreases. The importance of centennial variance in the Guaymas Basin is consistent with previous work identifying centennial variance in upwelling intensity (Peterson et al., 1991) and precipitation (record by Haug et al., 2001, analysis of variance by Poore et al., 2003) in the Cariaco Basin, and a lake record from the Yucatan Penninsula (Hodell et al., 2001). Poore et al. (2003) also observe important centennial variance in *G. Sacculifer* abundance

37

record, interpret changes in advection of Caribbean waters into the Gulf of Mexico, and attribute pervasive Holocene centennial variance to solar forcing.

The onset of important decadal variance at ~2800 yr BP is likely related to the coincident major change in oceanographic conditions and ecosystem structure identified from the other geochemical proxy records. Several previous studies suggest an increase in ENSO intensity at ~2800 yr BP in this Guaymas Basin and ETNP (Barron et al., 2004; Haug et al., 2001; Clement et al., 2000), however the age model and data resolution in this study are insufficient to resolve ENSO variance.

Higher-frequency peaks in the Core P12 Ca:Ti record are also consistent with records of continental aridity Mesoamerica. Two periods of drought at ~1750 and ~1650 yr BP are identified from a bulk Ti record in the Cariaco Basin and are interpreted as a main factor contributing to the collapse of Maya civilization (Haug et al., 2003). Droughts in Mesoamerica are associated with southerly ITCZ position, and pluvial periods with more northerly ITCZ position. Lachniet et al. (2017) presented a precisely dated high-resolution reconstruction of precipitation in Mesoamerica using speleothems from southwestern Mexico, and focused on identifying transitions from drought to pluvial conditions including transitions at ~1650 and ~1500 yr BP. The Core P12 age model is insufficient to resolve these droughts with confidence, however two peaks in the Core P12 Ca:Ti ratio record are identified at ~1675 and ~1525 yr BP. High Ca:Ti indicates high coccolith production in the Guaymas Basin, which is associated

with weak winds, stratified conditions, a northerly mean ITCZ position, and wet conditions. More generally, the records presented here characterize the period from 2800yr BP to present as a time of southerly mean ITCZ position and relatively dry conditions consistent with droughts.

6. Conclusions

1. The application of radiocarbon dating techniques in conjunction with the visual layer counting method reveals an apparent coretop age of ~1300 yr BP, and a discrepancy of ~1200 years between the two techniques. It is concluded that most or all of the ~1200 year discrepancy between dating methods can be explained by erosion or patchy deposition of couplets. This result is important for future paleoclimate studies, suggesting that caution must be exercised in the use of layer counting to date sediments in geologically active settings such as the Gulf of California.

2. The Core P12 $\delta^{15}N$, TOC:TN, TC:TN, weight percent nitrogen, PC 1, and Ca:Ti records resolve a major change in oceanographic conditions and ecosystem structure at 2800 yr BP.   The period prior to 2800 yr BP is characterized by a higher contribution of coccoliths to export production, which suggests an oceanographic regime marked by northerly ITCZ position, weak winds, a

stratified water column, and pluvial conditions on the continent. After 2800 yr

BP, conditions in the Guaymas basin changed to reflect a more southerly mean

ITCZ position, with stronger northwest winds, intense upwelling, high siliceous

productivity, sparse coccolith abundance, and higher aridity (Fig. 7). The

concurrent $0.63‰$ change in $\delta^{15}N$ indicates lower rates of denitrification and

increased ventilation in the Guaymas Basin after at 2800 yr BP. This change in

denitrification and anoxia is consistent with the increased seasonal upwelling

intensity suggested by the other geochemical records from Core P12, and

confirms the 2800 yr BP change recorded in DSDP Hole 480 (Barron et al., 2004).

3. Spectral analysis of Ca:Ti and PC 1 records shows centennial variance

at with important peaks at ~800, ~500, ~170, and ~120 year periodicities

throughout the record, and decadal variance with important peaks at ~100 and

~70 year periodicities only after 2800 yr BP.

Supplementary Text

1   Stable Isotope Data

1.1 Correction of Archive-half $\delta^{15}N$ data.

Core P12 was split into two halves upon collection. The working half (W-half) was sampled shipboard and samples were frozen immediately, whereas the archive half (A-half) remained unrefrigerated and was not sampled and frozen until ~ 2 years later. For this study, the W-half of the core was not available, so analyses were performed on the 87 available freeze-dried W-half samples. 99 additional new samples were taken from the A-half of the core in order to increase the total sampling resolution for the $\delta^{15}N$ record between 300cm and 100cm depth (Appendix 1). Analysis of these new data revealed a significant offset between W- and A- half $\delta^{15}N$ values (mean A-half $\delta^{15}N$ is ~1‰ lower than W-half $\delta^{15}N$ from similar depth interval).

An additional set of new samples were taken from the A-half, corresponding exactly to existing samples from the same depth in the W-half, with the goal of comparing matching samples from each half of the core directly. This set of 32 samples was analyzed with samples from the W-half run sequentially alongside samples from the same depth in the A-half, in an attempt to measure the magnitude of offset between the two halves of the core. A-half and W-half samples were run in alternating order through the Elemental Analyzer to avoid possible drift effects. The amount of offset between the W and

A-half samples appears vary with depth in the core, ranging from >1.5‰ at the top of the re-sampled interval (100cm depth) to <0.5‰ at ~300 cm depth (Fig. S4).

It is hypothesized that microbially mediated diagenetic activity in the W-half of the core was halted completely upon shipboard sampling and freezing, whereas diagenetic changes in the A-half were allowed to continue ~2 years longer, until recent sampling and freezing for this study. In fact, alteration of the A-half core may have been accelerated compared to *in situ* alteration due to the change in ambient conditions from the seafloor sediment pile to storage where the A-half was exposed to higher temperatures and oxygenation. This microbially mediated alteration probably affected the labile portion of N in the sediment organic material disproportionately, thus reducing the $\delta^{15}N$ values.

In order to correct this offset between W- and A-half samples, two data sets were used to establish correction factors averaged across four 50cm segments of the interval of interest. These segments were defined as 90-140cm, 140-190cm, 190-240cm, and 240-290cm, and the correction factors were calculated as the difference between the mean W-half $\delta^{15}N$ value and the mean A-half $\delta^{15}N$ value for each 50cm bin. A correction factor was calculated for each 50cm bin based on the entire set of $\delta^{15}N$ data from any depth within the 50cm interval, resulting in correction factors of 1.38‰, 0.90‰, 0.67‰, 0.50‰, respectively. A similar set of correction factors was calculated using only differences between the means of A-half and W-half samples taken from

42

identical depths, resulting in similar correction factors of 1.92‰, 0.99‰, 0.81‰, and 0.39‰, respectively. The final correction factor which has been applied to all A-half $\delta^{15}N$ data for this study is the mean of two correction factors calculated for each 50cm depth interval: 1.65‰, 0.94‰, 0.74‰, and 0.45‰, respectively (Fig. S4).   The corrected data, along with all other data is available in the associated supplementary file "Supplementary_File_1(data).xlsx".

1.2 $\delta^{13}C$ data

$\delta^{13}C$ values were measured on the organic fraction (see Methods in main text) (Fig. S3). The main reason for measuring $\delta^{13}C$ was to characterize the organic matter in Core P12 and detect any terrestrial organic matter (TOM) that may have been deposited by eolian input to the study site. The observed mean $\delta^{13}C$ of -20.7‰ suggests little to no contribution of TOM to the core (refer to discussion in main text). Although $\delta^{13}C$ organic increases downcore from -20.74‰ after 2800 ybp to -20.62‰ before 2800 ybp (p <0.0494 this 0.12‰ change is not interpreted as a paleoceanographic proxy record, because the observed difference is well within the 0.2‰ precision of the measurements.

1.3 NMAR

Measured dry bulk density of 0.2157 g/cm^3 was used to calculate NMAR following the formula:

NMAR g/cm^2/year = (wt%N)*(dry bulk density g/cm^3)*(sedimentation rate cm/year)

NMAR was determined using two different methods of calculating sedimentation rate: [14]C age-model derived sedimentation rate, and varve counting derived sedimentation rate (Fig. S5). However, changes in N cannot be accurately captured by either method of calculating NMAR, because missing sediment due to erosion events is thought to cause extreme variability in sedimentation rate, which dominates any "true" N signal. Therefore, bulk weight percent Nitrogen is considered rather than NMAR.

2 210Pb Dating

The radionuclide ^{210}Pb was analyzed by Peter Swarzenski at the USGS in Santa Cruz, CA. 13 samples from the upper 25cm of Core P12 were measured using gamma spectrometric methods after Swarzenski (2014). Excess Pb210 is observed in the upper 25cm of core P12, but does not exhibit the classic exponential decay with depth profile (Fig. S6). Rather, observed excess Pb210 varies stochastically between 1 and 4.5 dpm/g. It has been shown that radionuclide scavenging in the Guaymas Basin can vary with ENSO intensity (Smoak et al., 1998). Because ^{210}Pb lacks an exponential decay profile, and therefore cannot give a meaningful chronology for Core P12, can vary with

factors other than age, and disagrees with radiocarbon dates for Core P12, it is not interpreted here.

3 XRF data and Principle Component Analysis

In lieu of relying on traditional elemental ratios as paleoproxies, Principle Component Analysis (PCA) was performed on the full set of trace metal data from Al to Ba. The rationale behind this approach is that principle components that are influenced significantly by variability in water content should show a high z-score with elements common in seawater (S, Br, and Cl). Indeed, principle components 2, 3 and 4, show strong relationships to S, Br, and Cl, and are therefore interpreted to be strongly influenced by water content and water film thickness. The record of the 4 main principle components is reproduced here for reference (Fig. S8).

4 Other Statistical Analysis

T-tests were performed using an algorithm available at graphpad.com. The Pearson product moment correlation coefficient (subsequently referred to as "correlation coefficient") was calculated using the PEARSON function in Microsoft Excel, and indicates the extent of linear correlation between two data sets. Linear interpolation and re-sampling of data sets as well as spectral and

cross-spectral analyses were performed in the program Analyseries, which can be accessed at http://www.lsce.ipsl.fr/.

5   Smear Slide Analysis Methods

Samples were taken from the archive half of the core using a wooden toothpick or ~1cm wide glass slide to sample sediment. Samples taken with a toothpick targeted individual lamina from discrete intervals chosen to match peaks in the Ca:Ti record. Separate samples were taken from neighboring sets of light and dark lamination in order to characterize lithological differences between layers. In other intervals, a glass slide was used to scrape a 1cm swath of sediment from the core. This sediment was then mixed thoroughly before being fixed to a smear slide, in order to match the resolution of stable isotope data which were measured on bulk samples that integrate sediment across ~10 varves, or roughly 1cm core depth.

Finished smear slides were divided into a grid of 36 squares of equal size, and dice rolls were used to randomly select 3 squares to replicate counts on each slide. Percent cover was estimated for 11 categories: blank space, pennate diatoms, whole centric diatoms, fragmented centric diatoms, radiolarians, calcium carbonate, silicoflagellates, coccoliths, clay minerals, opaques, and silt-to-sand sized siliciclastics. The primary result of smear slide analysis was a strong relationship between percent cover coccolithophores and Ca:Ti ratio,

which forms the basis for the argument that Ca:Ti ratio can be used as a proxy record for coccolithophore production/preservation in the Guaymas Basin. Coccoliths were observed to make up a much higher percent cover of smear slides from intervals of high Ca:Ti ratio, with mean percent cover ranging from 10% to 30% for these intervals (Fig. 6). Magnified photographs of smear slides clearly show that the sediment is dominated by pennate and centric diatoms (and fragments), whereas coccoliths, which are only visible under cross-polarized light, are generally sparse (Fig. S7).

Figure 1. Bathymetric map of the Guaymas Basin, central Gulf of California, modified from Mortera (2014) with permission. Location of Core P12 is indicated by a red star (27° 52.1129' N by 111° 41.5062' W), nearby DSDP Hole 480 is shown by a black dot, and the approximate location of the Line B seismic reflection profile from DSDP initial report "5. Guaymas Basin Slope: Sites 479 and 480" is shown by a white dotted line. The extent of the Yaqui River alluvial fan is outlined in dotted white: Core P12 does not receive alluvial input from the Yaqui River.

Core P12

Yaqui River Fan

50 KM

-200
-600
-1100
-1500
-1900
m

49
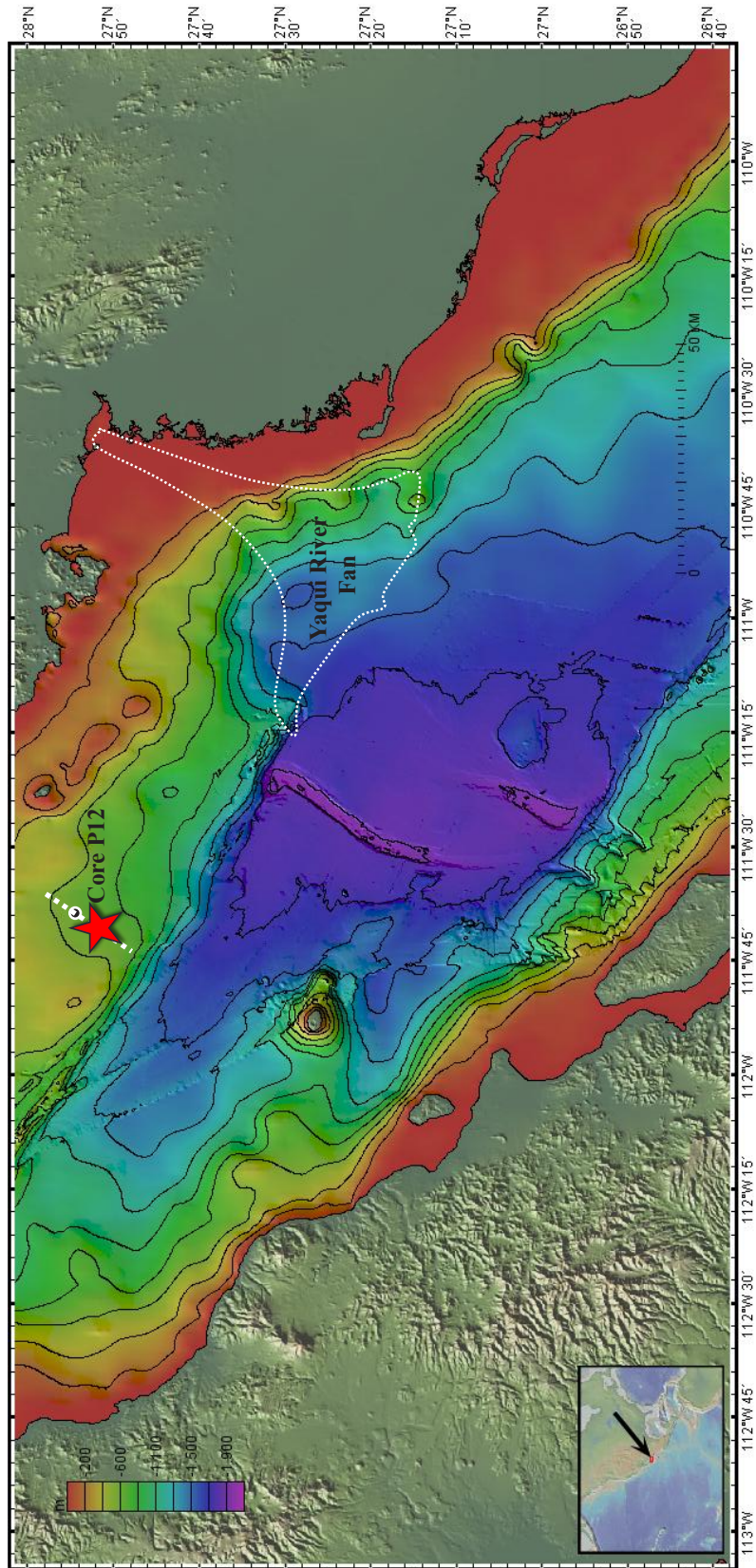
Figure 2. A) Age-depth relationship for Core P12 radiocarbon dates, and layer counting chronology. Radiocarbon dates indicate that the coretop is ~1300-years-old, and that the Core P12 record represents ~2800 years of accumulation, whereas layer counting suggests only ~1600 years. B) The difference between the radiocarbon and layercounting age-depth curves represent "missing laminae" absent from this record due to erosion or patchy deposition.

A

~1200-year
discrepancy

~1300-year-old
coretop

= radiocarbon dates
= layercounting

Age (yr BP)

Depth in core (cm)

B

= sigma 2 error

= age difference between C14 and layer counting

Age Difference (yr BP)

Depth in core (cm)

51
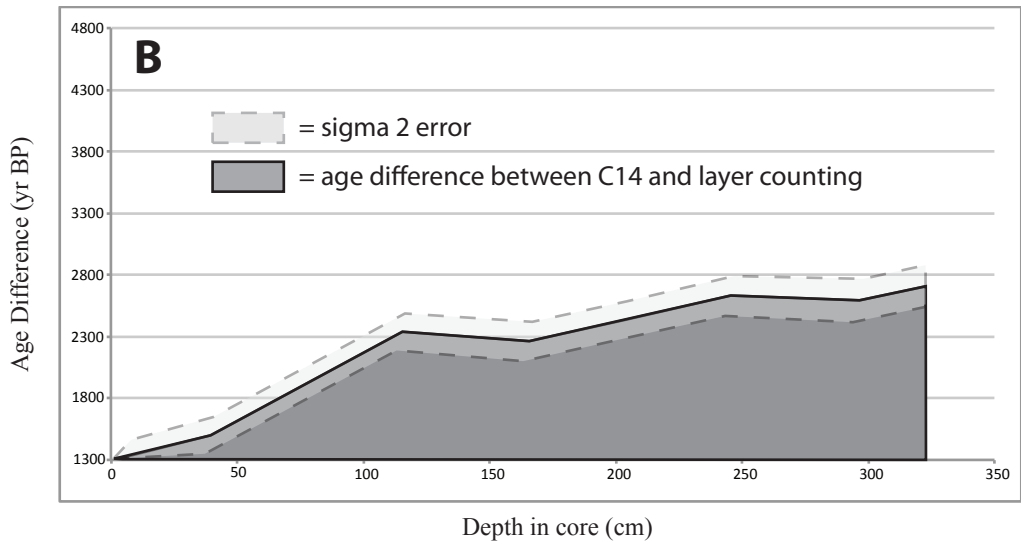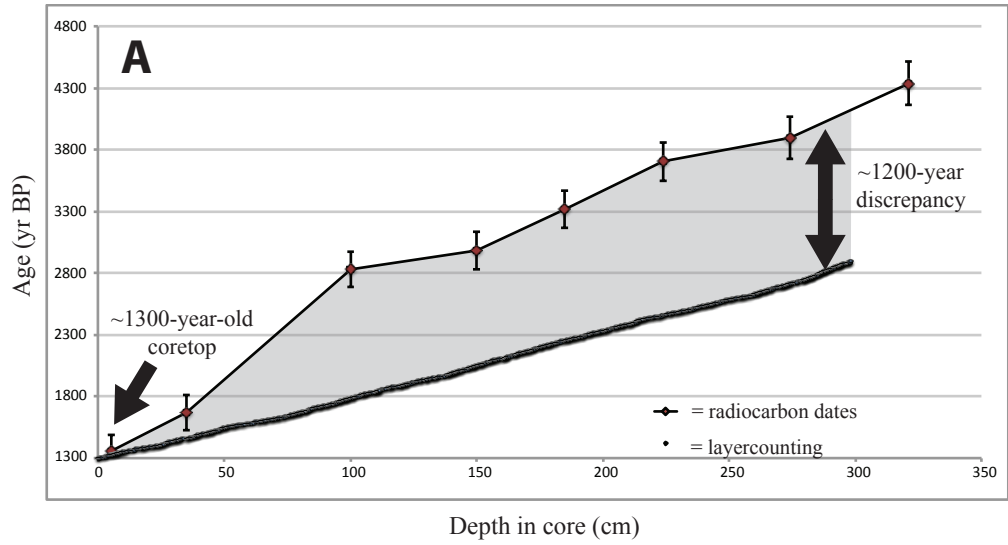
Figure 3. Core P12 Ca:Ti, d15N, C:N organic, C:N bulk, and PC 1 (eolian) plotted against depth (cm). Black triangles on the x axis represent depths where radiocarbon dates were measured, with error bars. Breaks in XRF records at core section-breaks are an artifact of the core scanning process.
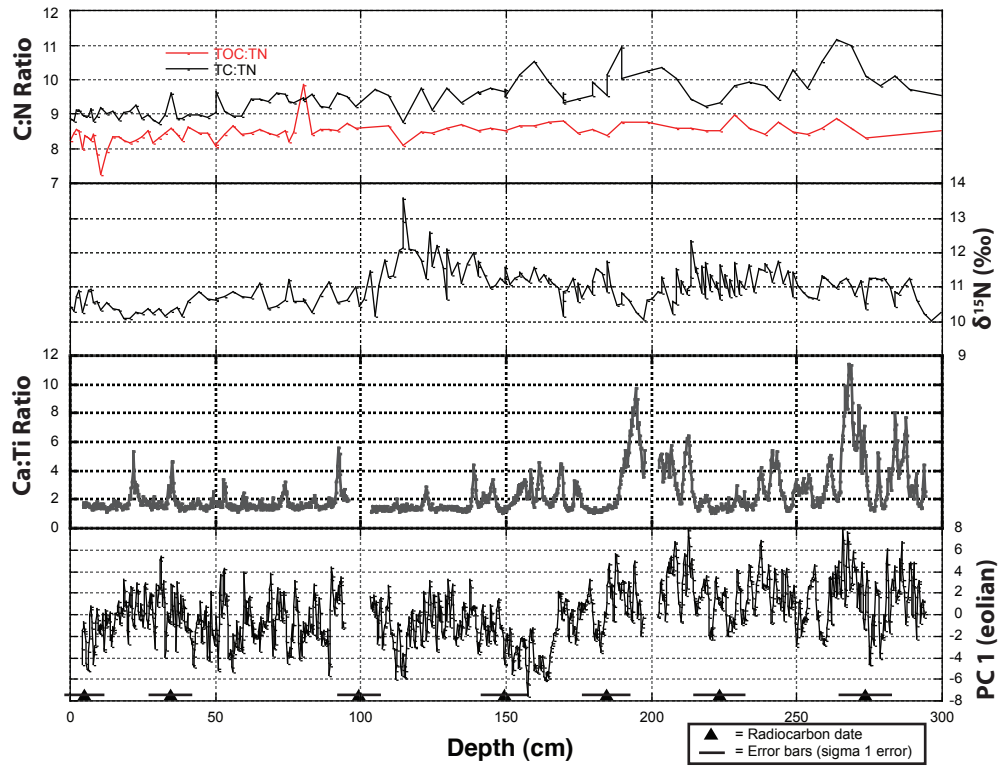
Figure 4. ~25cm section of the high resolution core photographs used to perform visual layercounting (scale in mm). Magnified insert (right) shows example of technique used to mark the center of each light colored lamination.
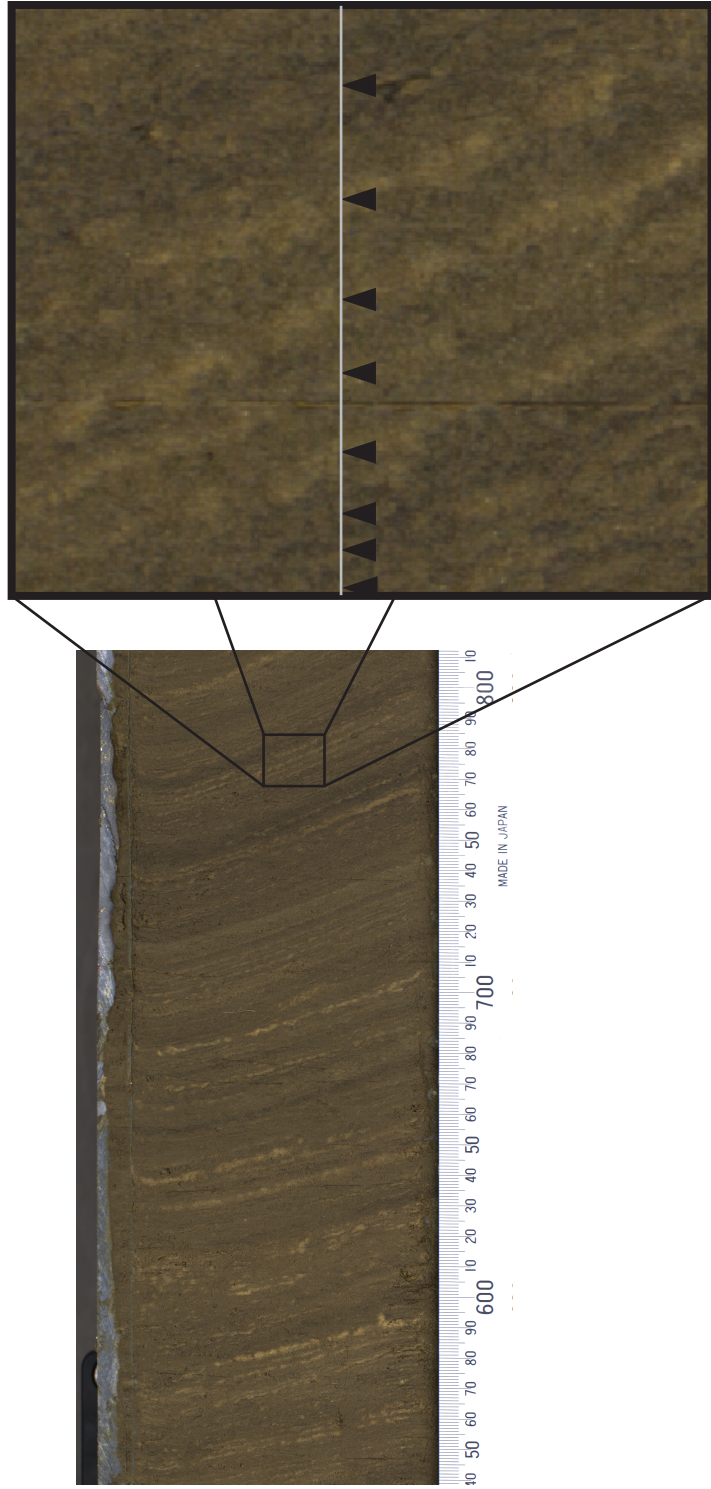
Figure 5. Principle component 1 (PC 1) accounts for 33% of variance, and is heavily influenced by K, Fe, Ti, Al, and Sr, elements with a detrital terrigenous source. Because Br, Cl, and S exert only a very weak influence on PC 1 (-0.014 and -0.143, respectively), variations in water content are not likely to exert significant influence over PC 1.

		PC 1 (33%)
Detrital	K	0.350
Detrital	Fe	0.348
Detrital	Ti	0.320
Detrital	Al	0.311
Detrital	Sr	0.303
	Rb	0.293
Detrital	Zr	0.288
Biogenic	Si	0.261
	Zn	0.219
Biogenic	Ca	0.215
	Ba	0.205
Water	S	0.187
	Pb	0.119
	Y	0.100
	Cu	0.056
	Ga	0.051
	Te	0.032
	Mn	0.021
	Nb	0.006
	Cd	0.002
Water	Br	-0.015
	Bi	-0.015
	Mo	-0.029
	P	-0.047
	Cr	-0.049
Water	Cl	-0.143

Legend:
- = z-score > 0.3
- = z-score 0.2 - 0.3
- = z-score 0.1 - 0.2
- = z-score < 0.1

Axis labels: PC 1 — PC #1 (detrital); Age (yr BP)

Figure 6. High percent cover coccoliths in smear slide analysis (pie charts) coincide with peaks in Ca:Ti ratio, which is interpreted as a proxy for coccolith content, and is also related to TC:TN and TOC:TN.
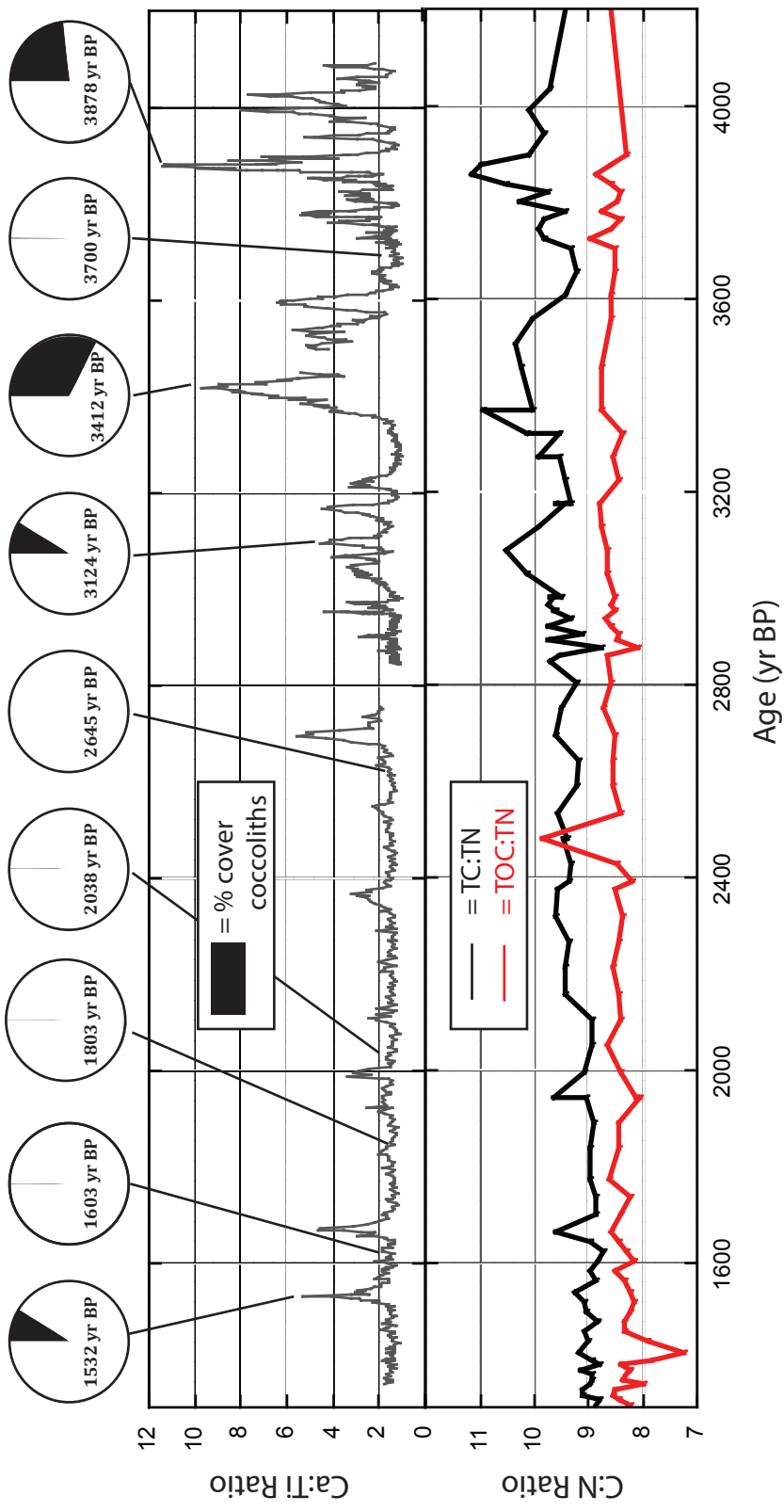
Figure 7. Core P12 records of Ca:Ti, δ^{15}N, TC:TN, TOC:TN, and weight % nitrogen plotted against age.   A major change at 2800 yr BP is observed, and a transition stratified to strong upwelling conditions driven by southward displacement of the ITCZ is interpreted. Pink stars indicate the radiocarbon dates used for age control on the record of Perez-Cruz (2013).

61
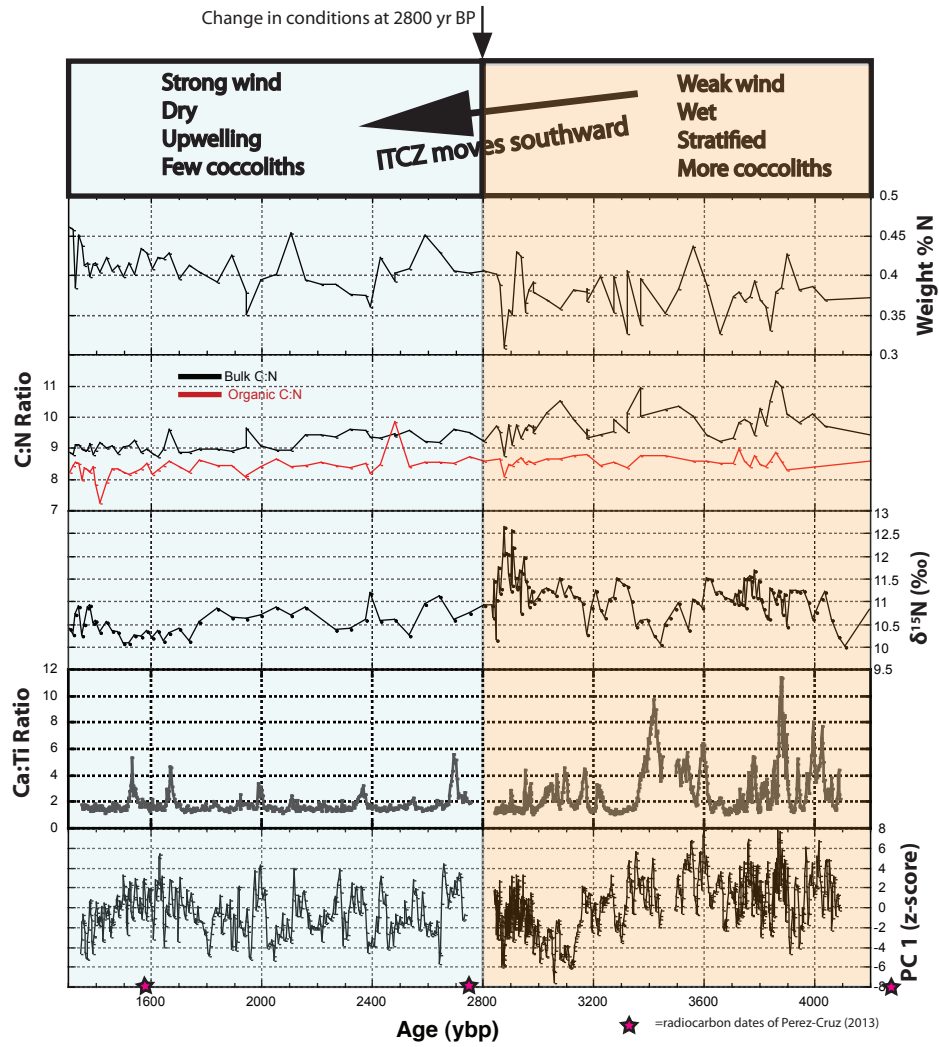
Figure 8. Spectra of variability in Ca:Ti and PC 1 records. Important peaks are indicated with periodicity in years, the % variability within core section in parenthesis, and the band of frequencies across which % variability was calculated in brackets.
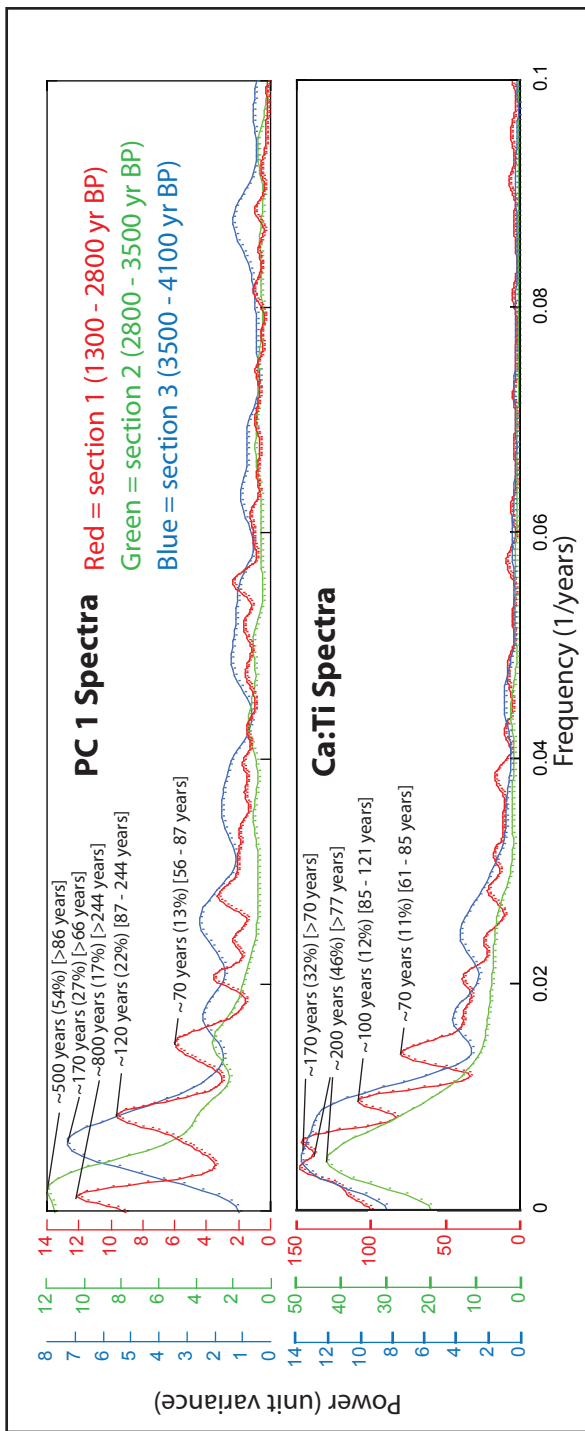
Supplementary Figure 1. Modified from Pares-Sierra et al. (2003). Seasonal surface winds in the Gulf of California during a.) December-January-February, b.) March-April-May, c.) June-July-August, and d.) September-October-November. Strong NW winds dominate the Guaymas Basin in the winter. Summer winds weaken and become NW to W, but do not reverse to SE as previously suggested. Star indicates the approximate location of Core P12.
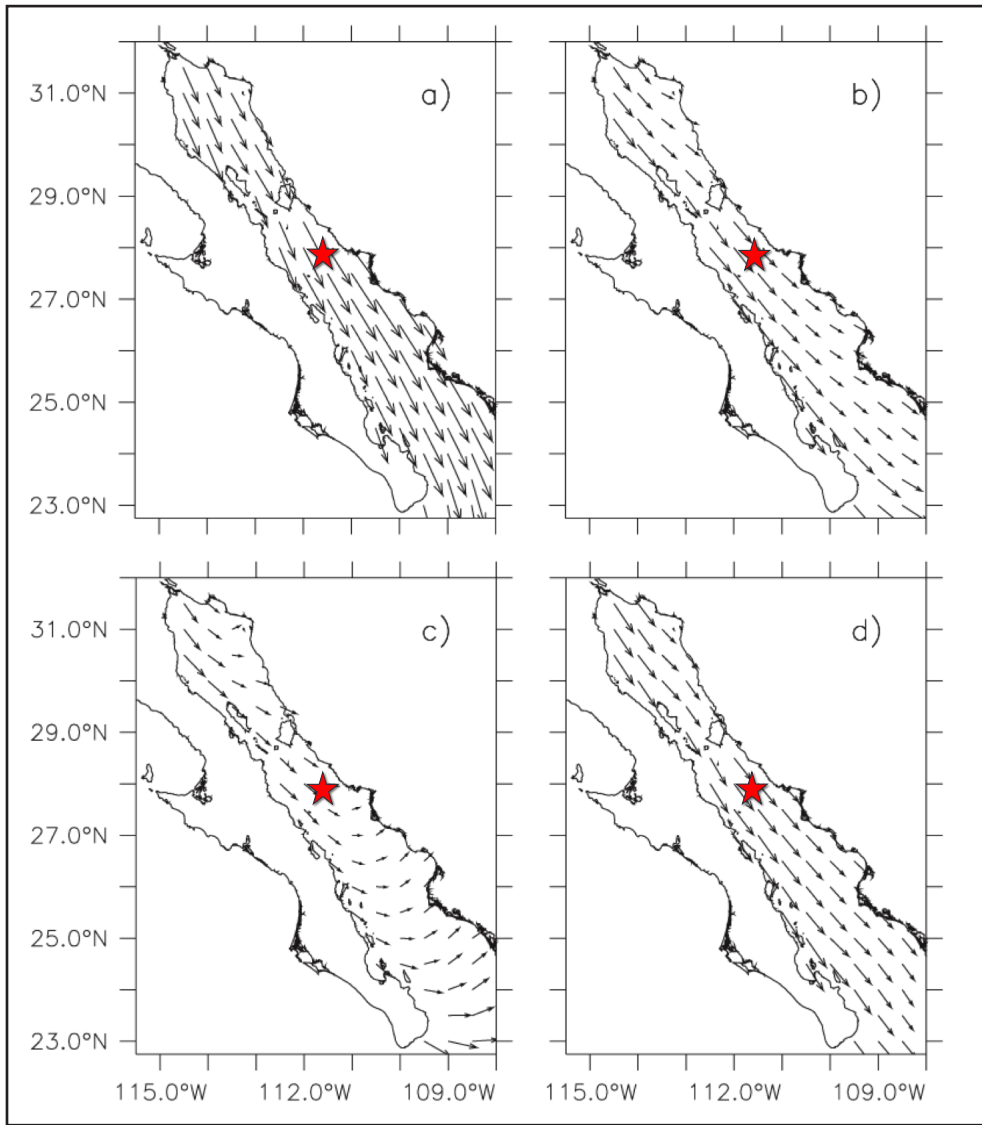
Supplementary Figure 2. Images reproduced from DSDP initial report "5. Guaymas Basin Slope: Sites 479 and 480". A) Seismic reflection profile of Line B with noticeable unconformaties traced with dashed line. Unconformities suggest slumping, soft sediment deformation, or mass-wasting events near the Core P12 site. B) Map showing position of DSDP hole 480 (black dot) and Core P12 (red star) relative to seismic line B (bold black line). C) Basin-scale interprative sketch of seismic profile, showing truncated, deformed, and folded beds near DSDP 480 and Core P12.
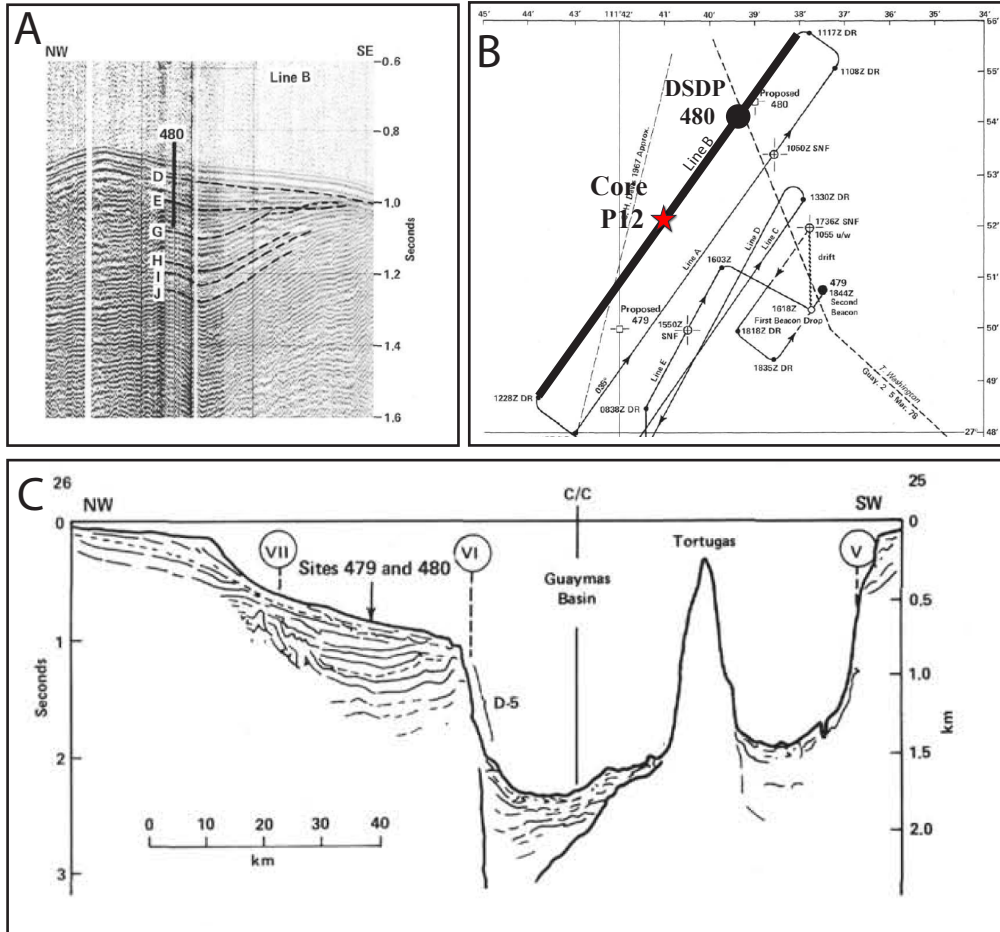
Supplementary Figure 3. δ13C organic changes from-20.62‰ before 2800 ybp to -20.74‰ after 2800 ybp (p < 0.0494). Because this 0.12‰ change is within the 0.2‰ precision of the stable isotope measurements, the trend is not interpreted. Mean δ13C values suggest marine organic matter.

δ¹³C
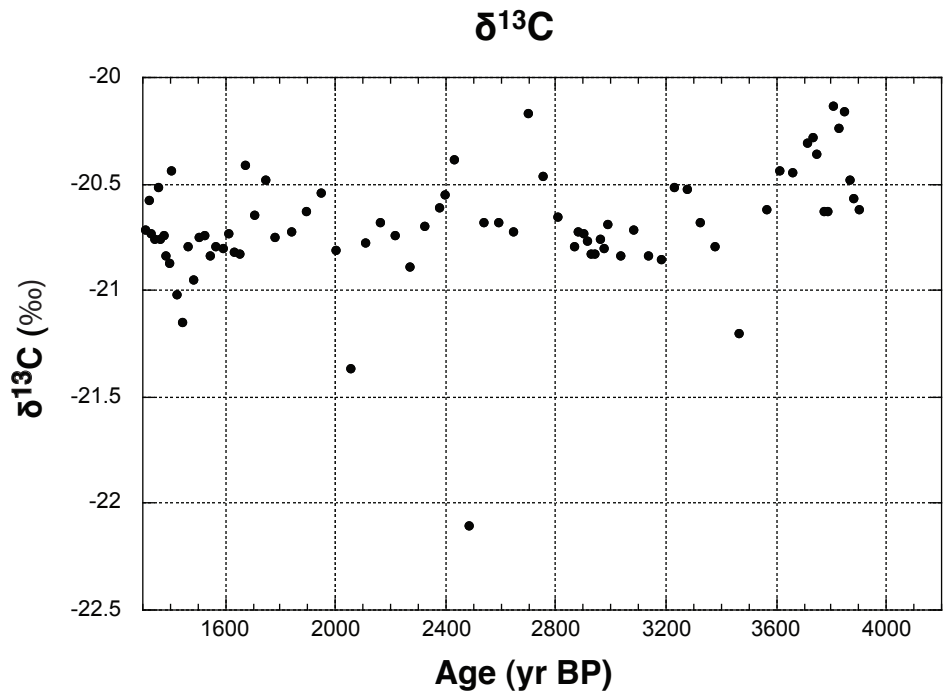
Supplementary Figure 4. A) Results of test-run where A-half and W-half samples from identical depths were compared. (B) Calculated difference between A-half and W-half samples for each of the four 50cm bins. Squares indicate differences calculated using only samples fromt the test-run where A-half and W-half samples from identical depths were directly compared, diamonds indicate differences calculated using binned means from the full set of all A-half and W-half data (not necessarily taken from identical depths). The final correction applied to A-half data is the average of results from these two methods for each 50cm bin.
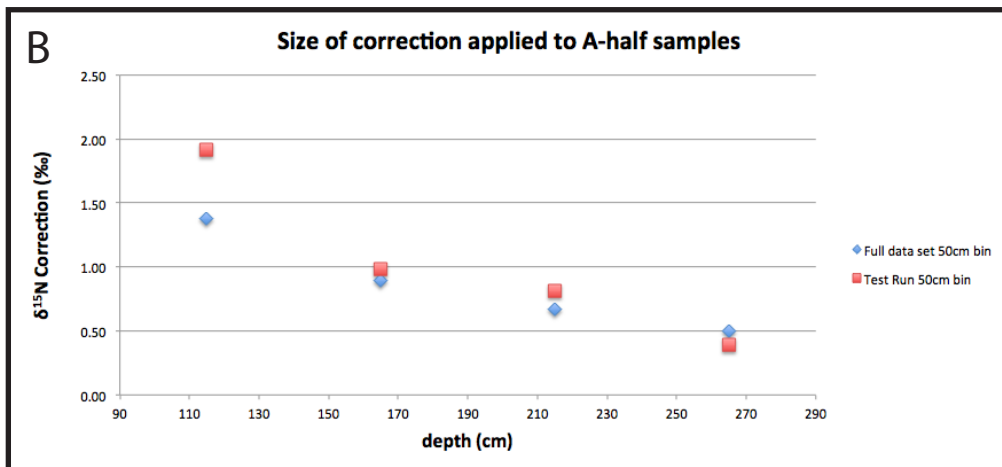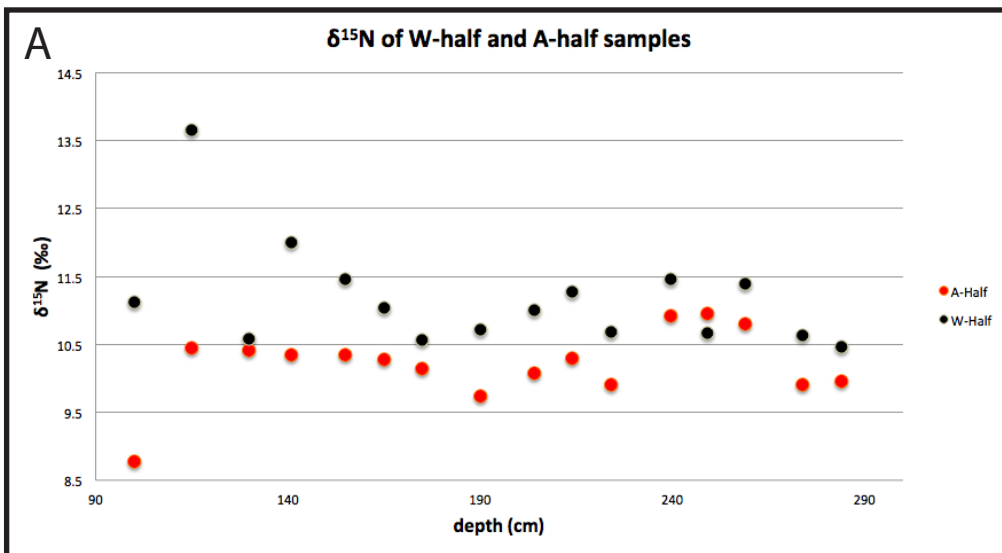
Supplementary Figure 5. Weight percent Nitrogen (top), NMAR calculated using a sedimentation rate derived from layer counting (center) and by radiocarbon (bottom). Due to the high variations in apparent sedimentation rate derived from either layercounting or 14C dating, any variability in NMAR is masked by variability in sedimentation rate. Therefore, wt% Nitrogen is considered a more useful paleoceanographic record than NMAR for Core P12.
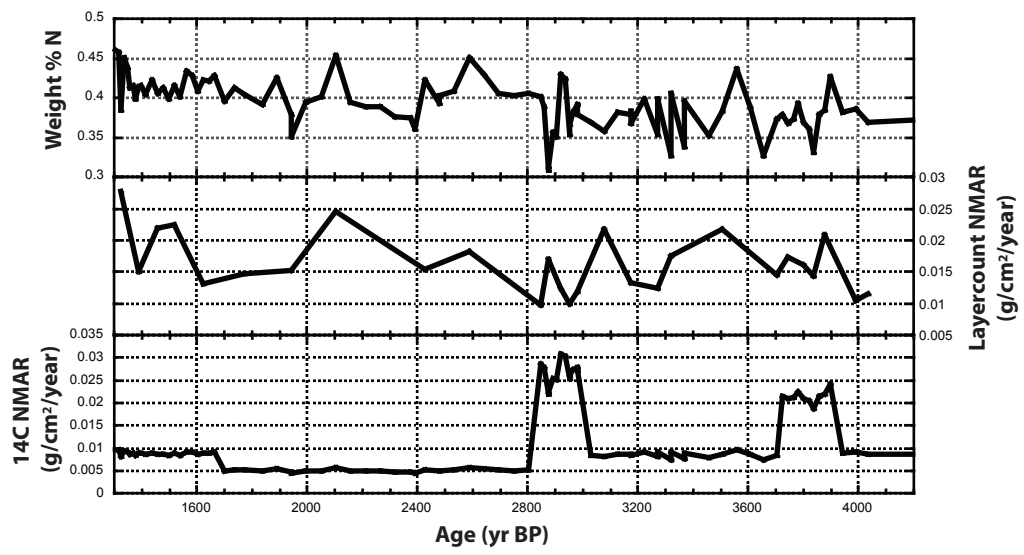
Supplementary Figure 6. Excess 210Pb is observed in the upper 25cm of core P12, but does not show a pattern of exponential decay that can be used to establish chronology.

Core P12 210Pb and 226Ra
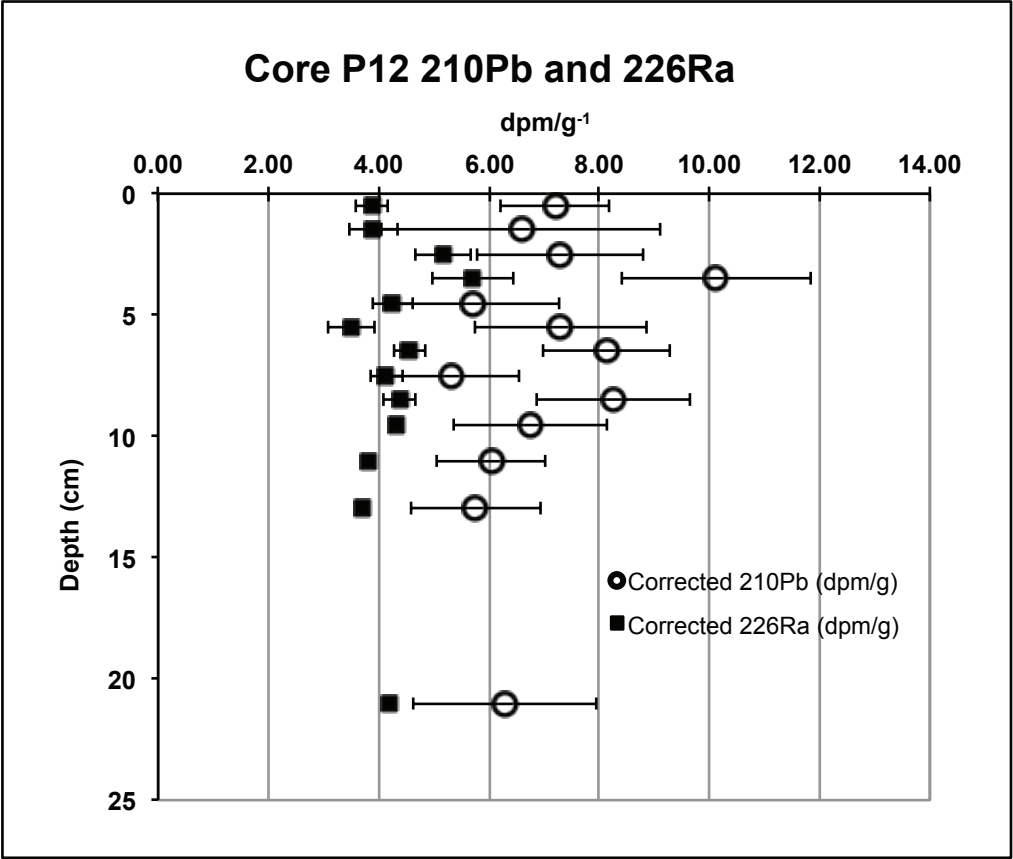
Supplementary Figure 7. Three smear slide images under normal light (left column) and cross-polarized light (right column). Distinctive pinwheel extinction patterns make the coccoliths apparent under cross-polarized light. An example of this pinwheel extinction is indicated by a black arrow in each image. Images A, B, E and F show 25x magnification, whereas Images C and D show 40x magnification.
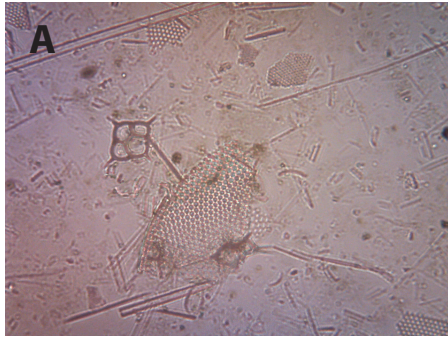
Normal Light   Cross-polarized Light
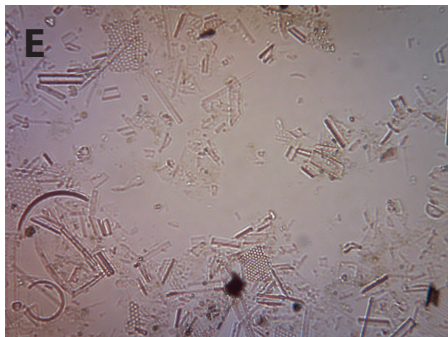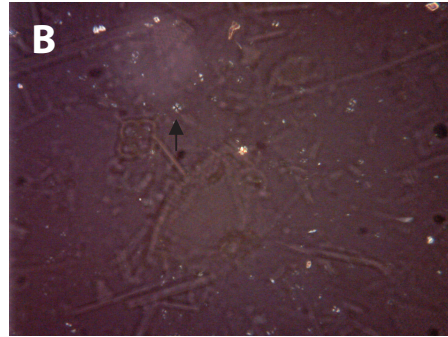
Supplementary Figure 8. Principle components 1-4 z-scores in table form, and plotted against depth in core (cm). Breaks in data are at transitions between ~1m core sections, where core casing and coverings prevent measurements for ~4.5cm.   PC 1 represents detrital input of K, Fe, Ti, Al, Sr, and Zr, and is not strongly influenced by any of the water content related elements (S, Br, Cl). PC 2, 3 and 4 are strongly influenced by S, Br, and Cl, and thus likely represent water content and porosity.
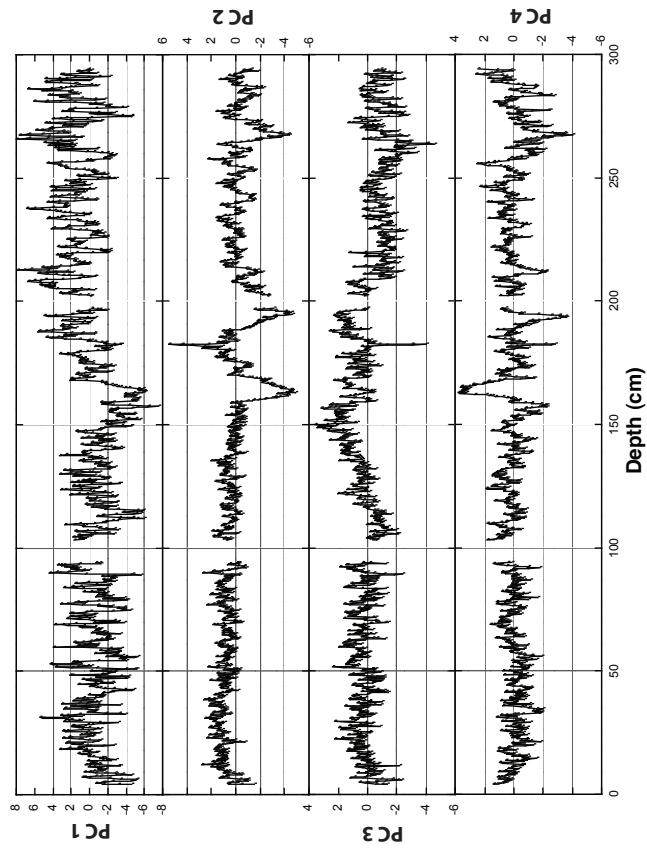
|		PC 1 (33%)	PC 2 (9%)	PC 3 (7%)	PC 4 (5%)
Detrital	K	0.350	0.077	-0.105	0.176
Detrital	Fe	0.348	0.086	0.106	0.118
Detrital	Ti	0.320	0.106	0.018	0.200
Detrital	Al	0.311	-0.064	-0.247	0.119
Detrital	Sr	0.303	-0.269	0.142	-0.360
Detrital	Rb	0.293	0.215	0.216	0.052
Detrital	Zr	0.288	0.192	0.274	0.038
Biogenic	Si	0.261	0.040	-0.540	0.051
Biogenic	Zn	0.219	0.135	0.197	-0.004
Biogenic	Ca	0.215	-0.479	-0.007	-0.446
	Ba	0.205	-0.058	0.246	-0.095
Water	S	0.187	0.117	-0.416	-0.278
	Pb	0.119	0.059	0.083	-0.002
	Y	0.100	0.125	0.151	-0.030
	Cu	0.056	0.073	0.134	-0.051
	Ga	0.051	0.004	0.081	0.010
	Te	0.032	0.123	-0.144	-0.169
	Mn	0.021	0.040	-0.007	-0.029
	Nb	0.006	0.173	-0.073	-0.074
	Cd	0.002	0.104	0.066	-0.002
Water	Br	-0.015	0.469	-0.274	-0.284
	Bi	-0.015	0.003	-0.013	0.068
	Mo	-0.029	0.035	-0.050	0.020
	P	-0.047	0.155	0.028	0.323
	Cr	-0.049	0.028	-0.094	0.177
Water	Cl	-0.143	0.471	0.198	-0.468

= z-score > 0.3
= z-score = 0.2 - 0.3
= z-score = 0.1 - 0.2
= z-score < 0.1

Supplementary Figure 9. Bold black line shows the simplified age model applied to XRF data for use in spectral analysis. This crude age model minimizes changes in sedimentation rate while remaining within 1 sigma error of each radiocarbon date.

Simplified Age Model for Spectral Analysis
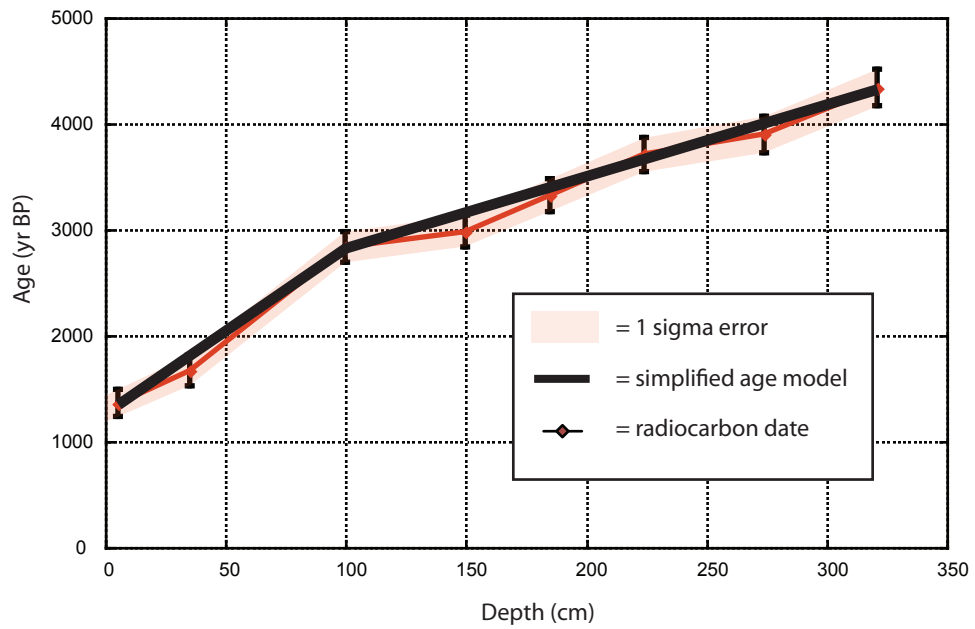
References

Agnihotri, R., Altabet, M. A., Herbert, T. D., and Tierney, J. E., 2008, Subdecadally resolved paleoceanography of the Peru margin during the last two millennia: Geochemistry Geophysics Geosystems, v. 9, p. 15.

Altabet, M., 2005, Isotopic tracers of the marine nitrogen cycle: present and past, *in* Volkman, J. K., ed., Marine Organic Matter: Biomarkers, Isotopes and DNA, Springer Berlin Heidelberg, p. 251-293.

Altabet, M. A., Francois, R., Murray, D. W., and Prell, W. L., 1995, Climate-related variations in denitrification in the Arabian Sea from sediment N-15/N-14 ratios: Nature, v. 373, no. 6514, p. 506-509.

Badan-Dangon, A., Dorman, C. E., Merrifield, M. A., and Winant, C. D., 1991, The lower atmosphere over the Gulf of California: Journal of Geophysical Research-Oceans, v. 96, no. C9, p. 16877-16896.

Barron, J. A., Bukry, D., and Bischoff, J. L., 2004, High resolution paleoceanography of the Guaymas Basin, Gulf of California, during the past 15000 years: Marine Micropaleontology, v. 50, no. 3-4, p. 185-207.

Barron, J. A., Bukry, D., and Dean, W. E., 2005, Paleoceanographic history of the Guaymas Basin, Gulf of California, during the past 15,000 years based on diatoms, silicoflagellates, and biogenic sediments: Marine Micropaleontology, v. 56, no. 3-4, p. 81-102.

Baumgartner, T., Ferreirabartrina, V., Schrader, H., and Soutar, A., 1985, A 20-year varve record of siliceous phytoplankton variability in the central Gulf of California: Marine Geology, v. 64, no. 1-2, p. 113-129.

Bopp, L., Le Quere, C, Heimann, M., and Manning, A. C., 2002, Climate induced oceanic oxygen fluxes: Implications for the contemporary carbon budget: Global Biogeochemical Cycles, v. 16, No. 2, p. 1022.

Bopp, L., Resplandy, L., Orr, J. C., Doney, S. C., Dunne, J. P., Gehlen, M., Halloran, P., Heinze, C., Ilyina, T., S√©f√©rian, R., Tjiputra, J., and Vichi, M., Multiple stressors of ocean ecosystems in the 21st century: projections with CMIP5 models: Biogeosciences, v. 10, no. 10, p. 6225-6245.

Brazel, A. J., and Nickling, W. G., 1986, The Relationship of Weather Types to Dust Storm Generation in Arizona (1965-1980): International Journal of Climatology, v. 6, p.

255-275.

Brazel, A. J., and S. Hsu, 1981, The Climatology of Hazardous Arizona Dust Storms, in T. L. Pewe, ed., Desert Dust: Origin, Characteristics and Effect on Man, Geological Society of America Special Paper 186, p. 293-303.

Brzezinski, M. A., 1985, The Si:C:N ratio of marine diatoms: interspecific variability and the effect on some environmental variables: Journal of Phycology, v. 21, no. 3, p. 347-357.

Clement, A. C., Seager, R., and Cane, M. A., 2000, Suppression of El Nino during the mid-Holocene by changes in the Earth's orbit: Paleoceanography, v. 15, no. 6, p. 731-737.

Dean, W., Pride, C., and Thunell, R., 2004, Geochemical cycles in sediments deposited on the slopes of the Guaymas and Carmen Basins of the Gulf of California over the last 180 years: Quaternary Science Reviews, v. 23, no. 16-17, p. 1817-1833.

Degens, E. T., 1969, Biogeochemistry of Stable Carbon Isotopes, *in* Eglinton, G., and Murphy, M. T. J., eds., Organic Geochemistry: Methods and Results: Berlin, Heidelberg, Springer Berlin Heidelberg, p. 304-329.

Deutsch, C., Berelson, W., Thunell, R., Weber, T., Tems, C., McManus, J., Crusius, J., Ito, T., Baumgartner, T., Ferreira, V., Mey, J., and van Geen, A., Centennial changes in North Pacific anoxia linked to tropical trade winds: Science, v. 345, no. 6197, p. 665-668.

Deutsch, C., Gruber, N., Key, R. M., Sarmiento, J. L., and Ganachaud, A., 2001, Denitrification and N-2 fixation in the Pacific Ocean: Global Biogeochemical Cycles, v. 15, no. 2, p. 483-506.

Drake K. M, Aiello I.W, Ravelo A. C (2014), *New method for the quantitative analysis of smearslides.* Abstract PP43B-1460 presented 2014 Fall Meeting, AGU, San Francisco, CA,15-19 Dec.

Einsele, G., and Kelts, K., 1982, Pliocene and Quaternary mud turbidites in the Gulf of California – sedimentology, mass physical-properties and significance: Initial Reports of the Deep Sea Drilling Project, v. 64, no. OCT, p. 511-528.

Emerson, S., and Hedges, J. I., 1988, Processes controlling the organic carbon content of open ocean sediments: Paleoceanography, v. 3, no. 5, p. 621-634.

Engel, A., Novoa, C. C., Wurst, M., Endres, S., Tang, T. T., Schartau, M., and Lee, C., No

detectable effect of CO2 on elemental stoichiometry of Emiliania huxleyi in nutrient-limited, acclimated continuous cultures: Marine Ecology Progress Series, v. 507, p. 15-30.

Haug, G. H., Gunther, D., Peterson, L. C., Sigman, D. M., Hughen, K. A., and Aeschlimann, B., 2003, Climate and the collapse of Maya civilization: Science, v. 299, no. 5613, p. 1731-1735.

Hedges, J. I., W. A. Clark, P. D. Quay, J. E. Richey, A. H. Devol, and U. de M. Santos, 1986, Compositions and fluxes of particulate organic material in the Amazon River: Limnology and Oceanography, v. 31, p. 717-738.

Hendy, I. L., Dunn, L., Schimmelmann, A., and Pak, D. K., Resolving varve and radiocarbon chronology differences during the last 2000 years in the Santa Barbara Basin sedimentary record, California: Quaternary International, v. 310, p. 155-168.

Hennekam, R., and de Lange, G., 2012, X-ray fluorescence core scanning of wet marine sediments: methods to improve quality and reproducibility of high-resolution paleoenvironmental records: Limnology and Oceanography: Methods, 10, 991-1003.

Hodell, D. A., Brenner, M., Curtis, J. H., and Guilderson, T., 2001, Solar forcing of drought frequency in the Maya lowlands: Science, v. 292, no. 5520, p. 1367-1370.

Karstensen, J., Stramma, L., and Visbeck, M., 2008, Oxygen minimum zones in the eastern tropical Atlantic and Pacific oceans: Progress in Oceanography, v. 77, no. 4, p. 331-350.

Kienast, M., 2000, Unchanged nitrogen isotopic composition of organic matter in the South China Sea during the last climatic cycle: Global implications: Paleoceanography, v. 15, no. 2, p. 244-253.

Lachniet, M. S., Asmerom, Y., Polyak, V., and Bernal, J. P., Two millennia of Mesoamerican monsoon variability driven by Pacific and Atlantic synergistic forcing: Quaternary Science Reviews, v. 155, p. 100-113.

Larson, R. L., Bathymetry, magnetic anomalies, and fracture zone trends in the Gulf of California, Geol. Soc. Amer. Bull., 83, 3345- 3360, 1972.

Lavin, M. F., and Marinone, S. G., 2003, An overview of the physical oceanography of the gulf of California, Nonlinear Processes in Geophysical Fluid Dynamics: A Tribute to the Scientific Work of Pedro Ripa, 173-204 p.

Liu, Z. H., Altabet, M. A., and Herbert, T. D., 2005, Glacial-interglacial modulation of eastern tropical North Pacific denitrification over the last 1.8-Myr: Geophysical Research Letters, v. 32, no. 23.

Liu, Z. H., Altabet, M. A., and Herbert, T. D., 2008, Plio-Pleistocene denitrification in the eastern tropical North Pacific: Intensification at 2.1 Ma: Geochemistry Geophysics Geosystems, v. 9.

Moore, D. G., 1973, Plate-edge deformation and crustal growth, Gulf of California structural province: Geological Society of America Bulletin, v. 84, no. 6, p. 1883-1905.

Pares-Sierra, A., Mascarenhas, A., Marinone, S. G., and Castro, R., 2003, Temporal and spatial variation of the surface winds in the Gulf of California: Geophysical Research Letters, v. 30, no. 6, p. 4.

Pearson, A., Seewald, J. S., and Eglinton, T. I., 2005, Bacterial incorporation of relict carbon in the hydrothermal environment of Guaymas Basin: Geochimica Et Cosmochimica Acta, v. 69, no. 23, p. 5477-5486.

Perez-Cruz, L., 2013, Hydrological changes and paleoproductivity in the Gulf of California during middle and late Holocene and their relationship with ITCZ and North American Monsoon variability: Quaternary Research, v. 79, no. 2, p. 138-151.

Peterson, L. C., Overpeck, J. T., Kipp, N. G., and Imbrie, J., 1991, A high-resolution late Quaternary upwelling record from the anoxic Cariaco Basin, Venezuela: Paleoceanography, v. 6, no. 1, p. 99-119.

Pewe, T. L., E. A. Pewe, R. H. Pewe, A. Journaux and R. M. Slatt, 1981, Desert Dust: Characteristics and rates of deposition in central Arizona, U.S.A., in Pewe, ed., Desert Dust: Origin, Characteristics and Effect on Man, Geological Society of America, Special Paper 186, p. 169-190.

Pichevin, L., Ganeshram, R. S., Reynolds, B. C., Prahl, F., Pedersen, T. F., Thunell, R., and McClymont, E. L., 2012, Silicic acid biogeochemistry in the Gulf of California: Insights from sedimentary Si isotopes: Paleoceanography, v. 27, p. 14.

Poore, R. Z., Quinn, T. M., and Verardo, S., 2004, Century-scale movement of the Atlantic Intertropical Convergence Zone linked to solar variability: Geophysical Research Letters, v. 31, no. 12.

Pride, C., Thunell, R., Sigman, D., Keigwin, L., Altabet, M., and Tappa, E., 1999, Nitrogen isotopic variations in the Gulf of California since the last deglaciation: Response to global climate change: Paleoceanography, v. 14, no. 3, p. 397-409.

Robinson, R. S., Kienast, M., Albuquerque, A. L., Altabet, M., Contreras, S., Holz, R. D., Dubois, N., Francois, R., Galbraith, E., Hsu, T. C., Ivanochko, T., Jaccard, S., Kao, S. J., Kiefer, T., Kienast, S., Lehmann, M. F., Martinez, P., McCarthy, M., Mobius, J., Pedersen, T., Quan, T. M., Ryabenko, E., Schmittner, A., Schneider, R., Schneider-Mor, A., Shigemitsu, M., Sinclair, D., Somes, C., Studer, A., Thunell, R., and Yang, J. Y., A review of nitrogen isotopic alteration in marine sediments: Paleoceanography, v. 27, p. 13.

Silverberg, N., Aguirre-Bahena, F., and Mucci, A., Time-series measurements of settling particulate matter in Alfonso Basin, La Paz Bay, southwestern Gulf of California: Continental Shelf Research, v. 84, p. 169-187.

Sigman, D. M., Karsh, K. L., and Casciotti, K. L., 2009, Nitrogen Isotopes in the Ocean A2 - Steele, John H, Encyclopedia of Ocean Sciences (Second Edition): Oxford, Academic Press, p. 40-54.

Smoak, J. M., Moore, W. S., Thunell, R. C., and Shaw, T. J., 1999, Comparison of 234Th, 228Th, and 210Pb fluxes with fluxes of major sediment components in the Guaymas Basin, Gulf of California: Marine Chemistry, v. 65, no. 3,Äì4, p. 177-194.

Swarzenski, P. W., 2014, 210Pb Dating, Encyclopedia of Scientific Dating Methods: Dordrecht, Springer Netherlands, p. 1-11.

Thunell, R., Pride, C., Ziveri, P., MullerKarger, F., Sancetta, C., and Murray, D., 1996, Plankton response to physical forcing in the Gulf of California: Journal of Plankton Research, v. 18, no. 11, p. 2017-2026.

Thunell, R., Pride, C., Tappa, E., and Mullerkarger, F., 1993, Varve Formation in the Gulf-of-California - Insights from Time-Series Sediment Trap Sampling and Remote-Sensing: Quaternary Science Reviews, v. 12, no. 6, p. 451-&.

Thunell, R. C., 1998, Seasonal and annual variability in particle fluxes in the Gulf of California: A response to climate forcing: Deep-Sea Research Part I-Oceanographic Research Papers, v. 45, no. 12, p. 2059-2083.

White, A. E., Foster, R. A., Benitez-Nelson, C. R., Masque, P., Verdeny, E., Popp, B. N., Arthur, K. E., and Prahl, F. G., Nitrogen fixation in the Gulf of California and the Eastern Tropical North Pacific: Progress in Oceanography, v. 109, p. 1-17.